*Transactions of the Royal Society of Edinburgh: Earth Sciences,* **95**, 423–444, 2005 (for 2004)

# Palaeoproterozoic, rift-related, $^{13}C$-rich, lacustrine carbonates, NW Russia. Part II: Global isotope signal recorded in the lacustrine dolostones

V. A. Melezhik, A. E. Fallick and A. B. Kuznetsov

ABSTRACT: A comprehensive study of the ~2200-Ma-old Kuetsjärvi Sedimentary Formation (KSF), NW Russia, was undertaken to contribute to our understanding of palaeoenvironments associated with the global perturbation of the carbon cycle between 2330 and 2060 Ma. Closely spaced drill core samples ($n$=95) were obtained from a 150-m-thick unit deposited in rift-bound fluvial-deltaic and shallow-water lacustrine settings with a short-term invasion of sea water. Apart from a very few de-dolomitised samples, all other carbonate lithologies are represented by $C_{org}$-free, S-poor, quartz-rich dolostones, stromatolites and travertines which have high Sr concentrations (51–1069 ppm) and low Mn/Sr ratios (2·9 ± 2·1). The carbonate succession, excluding travertines, shows high $\delta^{13}C$ (+7·5 ± 0·6‰, $n$=95) with a limited variation (+5·8 to +8·9‰). Fluctuating $\delta^{18}O$ values (10·8–20·4‰) were overprinted during diagenesis, regional greenschist-grade and later retrograde metamorphism. Several short-term stratigraphic excursions of $\delta^{13}C$ were apparently governed by evaporation and $CO_2$ degassing combined with pulses of $^{12}C$-rich hydrothermal waters precipitating travertines. However, the $^{13}C$-rich nature of the dolostones reflects the global isotopic signal, which was modified in a shallow water lacustrine environment by evaporation, enhanced uptake of $^{12}C$ by cyanobacteria, and pene-contemporaneous oxidation and loss of organic material. The best proxies to $\delta^{13}C$ and $^{87}Sr/^{86}Sr$ of coeval sea water recorded in the KSF dolostones are likely to be around +5–6‰ and 0·70406, respectively. The study of the KSF has shown that circumspection is necessary when attempting to model the behaviour and evolution of the global C-cycle in Deep Time. Models which purport to explain global oceanic–atmospheric evolution without first adequately accounting for the possibility that many Precambrian carbonate deposits might be non-marine, or at least influenced by non-marine fluids, should be viewed with caution.

KEY WORDS: Carbon, dolomite, isotopes, oxygen, stromatolite, strontium.

The stable isotopic compositions of $C_{carb}$, $C_{org}$, S and Sr in the oceanic reservoir are, in general, relatively homogenous because their residence times are greater than the mixing times of the oceanic water mass. This is not the case for the bulk terrestrial sedimentary reservoir of these elements. However, carbon represents an unusual case because the oceanic and continental reservoirs have an interactive link through atmospheric $CO_2$. Correlation between marine and non-marine environments of deposition using carbon isotope chemostratigraphy has been demonstrated for the Palaeocene–Eocene boundary (Koch *et al.* 1992), where an isotope excursion of $\delta^{13}C_{carb}$ has been correlated between marine carbonates, palaeosol carbonates and mammalian tooth enamel. Morante *et al.* (1994) reported a similar link between marine and non-marine records for $\delta^{13}C_{org}$ at the Permian–Triassic boundary. These two examples demonstrate that a link between marine and non-marine carbon reservoirs existed in the past.

The Palaeoproterozoic is of particular interest for carbon isotope investigation because it is marked by one of the greatest positive $\delta^{13}C_{carb}$ excursions and the concomitant accumulation of stable free oxygen in the terrestrial atmosphere (Baker & Fallick 1989a, b; Karhu & Holland 1996). This excursion was originally recorded in the Lomagundi basin (Schidlowski *et al.* 1976), and lately, has been constrained between 2330 and 2060 Ma (Karhu 1993). Although the excursion has been best documented on the Fennoscandisn Shield (Baker & Fallick, 1989b; Yudovich *et al.* 1991; Karhu & Melezhik 1992; Karhu 1993; Tikhomirova & Makarikhin 1993; Akhmedov *et al.* 1993; Pokrovsky & Melezhik 1995; Melezhik & Fallick 1996), similar, 2330–2060 Ma, isotopically anomalous carbonate formations have been reported from other continents (reviewed in Melezhik *et al.* 1999).

Baker & Fallick (1989b) were the first to recognise the global nature of this phenomenon and suggested that the development of Palaeoproterozoic $^{13}C$-rich carbonates was caused by accelerated burial of reduced carbon with subsequent release of oxygen and perturbation of the terrestrial carbon cycle. However, despite the fact that the Palaeoproterozoic isotope excursion has global significance, the geological data necessary for understanding the mechanism responsible for $\delta^{13}C$ values as high as between +8 and +18‰ are not yet available (e.g. Melezhik & Fallick 1996). The true global background value of $\delta^{13}C$ for this period of time remains a subject for debate (Melezhik & Fallick 1997; Shields 1997; Buick *et al.* 1998; Melezhik *et al.* 1999; Bekker *et al.* 2001). $\delta^{13}C$ up to +28‰, recently reported from the Nash Fork Formation on the Wyoming Craton in the USA (Bekker *et al.* 2003), represents a further fundamental challenge if such values are to be interpreted as a global oceanographic signal.

Since Karhu & Melezhik (1992) reported $^{13}C$-rich carbonates from the ca. 2200 Ga Kuetsjärvi Sedimentary Formation (KSF) in the Northeast Transfennoscandian Belt (Fig. 1), this formation has become one of the main targets for C-isotope

https://doi.org/10.1017/S0263593300001152 Published online by Cambridge University Press

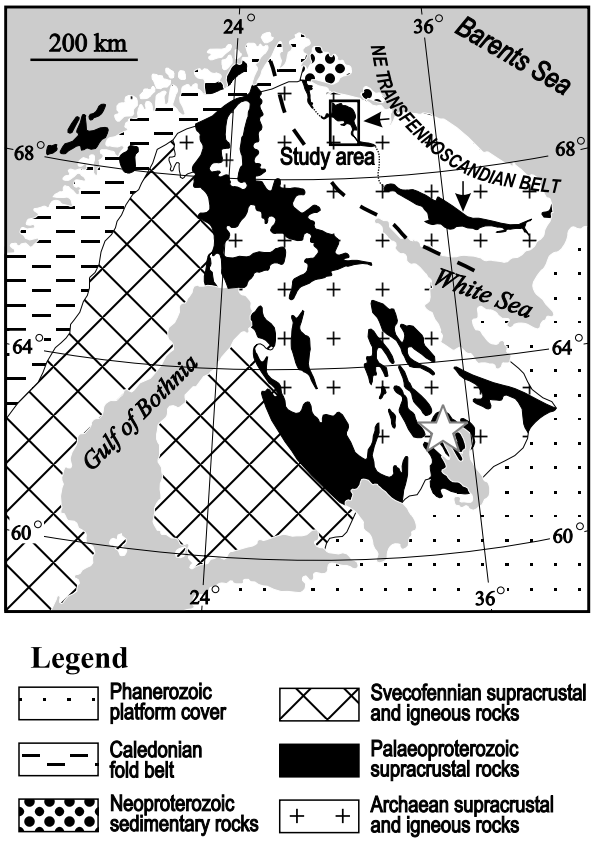


**Figure 1** Geographical and geological location of the study area. The star indicates the position of the Tulomozerskaya Formation. The dashed line shows the axis of the c. 2·0 Ga oceanic separation of the Fennoscandian Shield (Daly *et al*. 2001). For a detailed geological map of the Pechenga Greenstone Belt, see Melezhik & Fallick (2005).

investigations (e.g. Akhmedov *et al*. 1993; Pokrovsky & Melezhik, 1995; Melezhik & Fallick 1996, 2001; Melezhik *et al*. 2003). $^{13}$C-rich carbonates have been traced in the Northeast Transfennoscandian Belt over a distance of 1000 km (Fig. 1). The belt appears to be one of continuous geological structures with $^{13}$C-rich carbonate formations, and therefore, it has become a very important province for studying the spatial heterogeneity of $\delta^{13}$C records.

A companion paper (Melezhik & Fallick 2005) on the sedimentology, major element geochemistry and depositional environments of the KSF demonstrated a coastal and shallow-water lacustrine character for the sedimentary succession. The present paper describes the carbon, oxygen and strontium isotope geochemistry of these lacustrine carbonate rocks.

The objectives of the present paper are to describe and discuss: (1) carbon, oxygen and strontium isotope systematics; (2) metamorphic/diagenetic overprinting of carbon, oxygen and strontium isotope systems; (3) links between marine and non-marine carbon reservoirs; and (4) the significance of the KSF $\delta^{13}$C record for reconstructing the isotopic composition of Palaeoproterozoic sea water.

## 1. Sampling sites and material studied

The 120-m-thick KSF is one of the lower formations within the Pechenga Greenstone Belt in NW Russia (Melezhik & Fallick 2005). It is sandwiched between two, 2000-m-thick, subaerially deposited volcanic formations. Eleven units have been recognised in the KSF succession, and grouped into siliciclastic-dominated, mixed clastic–dolostone and dolostone-dominated units (Melezhik & Fallick 2005). The siliciclastic-dominated rocks form the lower portion of the KSF; the siliciclastic–dolostone units are developed throughout the formation, whereas the dolostone-dominated units are associated with the upper part of the succession (Fig. 2). Micritic dolostones, and micritic and sparry allochemical dolostones are the prevalent rocks, and they have been documented in all units. Microbial dolostones form the essential volume of units VII and X, and are sparsely developed in Unit VI (Fig. 2). Clastic rocks of Unit IV, as well as carbonate rocks of units VIII and X, are typical representatives of Palaeoproterozoic 'red beds'. Abundant travertine crusts have been documented throughout units VII and X (Melezhik & Fallick 2001).

In order to minimise the influence of recent weathering on the carbon and oxygen isotopes, all samples for the isotopic study were obtained either from drill-core material or from operating quarries. Most of the samples have been obtained from drill hole X (DHX), which was drilled in the central part of the Pechenga Belt and intersected the complete succession (Fig. 2). Samples have been collected from the depth interval from 267 to 395 m. Good drill-core recovery allowed high-density sampling through the entire formation. The use of drill cores enables accurate stratigraphic positioning of samples with respect to one another within the section. One hundred and eleven samples were obtained from drill-core material, with the density of sampling ranging from 0·1 to 1·0 m (0·5 m on average) within the carbonate succession. Ten sub-milligram microsamples for oxygen, carbon and strontium isotope analyses for detailed studies were acquired using an Ulrike Medenbach microcorer, which enables core diameters from 50 μm to several millimetres to be obtained with a maximum drilling depth of 1 mm. The microsamples were cored from 150-mm-thick polished sections stained by Alizarin-red.

## 2. Methods

Acid-soluble Ca, mg, Mn and Sr were analysed by ICP-AES at the Geological Survey of Norway using a Thermo Jarrell Ash ICP 61 instrument. The detection limits for Mg, Ca, Mn and Sr are 100, 200, 0·2 and 5 ppm, respectively. The total analytical uncertainty including element extraction (1σ) is ± 10% rel.

Whole-rock oxygen and carbon isotope analyses were carried out at the Scottish Universities Environmental Research Centre using the phosphoric acid method of McCrea (1950), as modified by Rosenbaum & Sheppard (1986) for operation at 100°C. Carbon and oxygen isotope ratios were measured on a VG SIRA 10 mass spectrometer. Calibration to international reference material was through NBS 19 and precision (1σ) for both isotope ratios is better than ± 0·2‰. Oxygen isotope data were corrected using the fractionation factor 1·00913 recommended by Rosenbaum & Sheppard (1986) for dolomites. The $\delta^{13}$C data are reported in per mil (‰) relative to V-PDB and the $\delta^{18}$O data in ‰ relative to V-SMOW.

Rb-Sr analyses were carried out at the Institute of Precambrian Geology and Geochronology of the Russian Academy of Sciences, St Petersburg, as specified in Gorokhov *et al*. (1995). The Rb and Sr concentrations were determined by isotope dilution. Rb isotopic composition was measured on a multi-collector MI 1320 mass spectrometer. Strontium isotope analyses were performed in static mode on a Finnigan MAT-261 mass spectrometer. All $^{87}$Sr/$^{86}$Sr ratios were normalised to a $^{87}$Sr/$^{86}$Sr of 0·1194 and measurements of the NIST SRM-987 run with every batch averaged 0·710246 ± 6 ($2\sigma_{mean}$, $n$=4). During the course of the study, the value obtained for the $^{86}$Sr/$^{88}$Sr ratio of the U.S.G.S. EN-1 standard was measured at 0·709181 ± 9 ($2\sigma_{mean}$, $n$=2).

https://doi.org/10.1017/S0263593300001152 Published online by Cambridge University Press

## 3. Results

One hundred and eleven drill-core samples were analysed for major and trace elements, and 96 samples for oxygen and carbon isotope ratios (Table 1). Strontium isotope ratios were obtained from 16 selected samples (Table 2).

### 3.1. Major element geochemistry

Most of the carbonate rocks studied are very impure. They are rich in clastic quartz and contain 0·5–53·5 wt.% $SiO_2$ (20 wt.% on average) (Melezhik & Fallick 2005). The quartzite-hosted lenses of carbonate rocks in units I–V are most enriched in $SiO_2$ (17–45 wt.%). The dolostone-dominated units VI–VII contain less $SiO_2$ (0·5–27 wt.%), whereas units IX–XI occupy an intermediate position (12–37 wt.%). The dolostones contain only 0·01–5·5 wt.% $Al_2O_3$ (1·5 wt.% on average), little $K_2O$ (0·5 wt.% on average) and are almost devoid of $Na_2O$ (0·1 wt.% on average).

$C_{org}$ concentrations in the dolostones and siliciclastic rocks are below detection limit of 0·1 wt.%. The average $S_{tot}$ content in the dolostones is $0{\cdot}01 \pm 0{\cdot}06$ ($n=25$) with fluctuation from 0·01 to 0·23 wt.%. The associated siliciclastic rocks contain 0·02–0·47 wt.% of $S_{tot}$ (Melezhik & Fallick 2005).

### 3.2. Mg/Ca ratios of carbonates

Most of the carbonate rocks are dolostones with an Mg/Ca ratio close to stoichiometric dolomite (Fig. 2, Table 1). The carbonate rocks hosted by siliciclastic units, and those located close to contacts with the overlying and underlying volcanic rocks are partially or entirely de-dolomitised (Mg/Ca=0·05–0·40). However, there are a few de-dolomitised rocks within the dolostone-dominated Unit VI (343·2–343·6 m) and within shear zones (290·5 m; Fig. 2).

### 3.3. Mn and Sr concentrations in carbonates

The rocks are relatively low in Mn (59–1838 ppm, $360 \pm 296$ ppm, $n=95$) and rich in Sr (51–1069 ppm, $174 \pm 183$ ppm, $n=100$). In the upper part of the succession, the Sr concentration increases upwards monotonously from 60 to 600 ppm, starting from 284·5 m (Fig. 3a). This increase correlates positively with the Mn concentration, although within a shorter interval, starting from 274 m (Fig. 3a). Although the overall data show no correlation between Mn and Sr concentrations ($r=0{\cdot}28$, $n=95$), there are two particular intervals in the succession where a significant positive correlation is observed. One ($r=0{\cdot}84$, $n=12$, >99·9%, if two samples are excluded; Fig. 4a) occurs in the quartzite-hosted lenses of de-dolomitised rocks of the lower part of the section (382·1–344·7 m; Fig. 3a). The other ($r=0{\cdot}85$, $n=17$, >99·9%; Fig. 4a) appears in the dolostones of the upper part of the section (272·7–268·0 m).

Although the overall data suggest a weak negative correlation between Sr concentrations and Mg/Ca ratios ($r=-0{\cdot}27$), the de-dolomitised varieties tend to be enriched in Sr (Table 1). If all the samples are divided into four groups based on the Mg/Ca ratios of <0·20, 0·20–0·40, 0·40–0·50 and ≥0·50, this corresponds to 288 ($n=5$), 194 ($n=6$), 188 ($n=20$) and 126 ppm ($n=64$) of Sr. This geochemical trend is consistent with a similar decrease in Mn concentration, i.e. 723, 706, 437 and 278 ppm. The quartzite-hosted carbonates show a negative correlation between Mn concentrations and Mg/Ca ratios ($r=-0{\cdot}49$; Fig. 4b).

There are four units in which the dolostones are relatively enriched in $Fe_2O_{3(tot)}$ with respect to the average value of 0·47 wt.%. These are Unit II (0·79 wt.% on average), Unit IV (1·33 wt.%), Unit VIII (1·10 wt.%) and Unit XI (1·33 wt.%).

### 3.4. Mn/Sr ratio in carbonates

The rocks are relatively low in Mn and rich in Sr, which results in a low Mn/Sr ratio (0·4–10, $2{\cdot}9 \pm 2{\cdot}1$, $n=95$, Fig. 2). The Mn/Sr>4 is a characteristic feature of the quartzite-hosted carbonates, tectonically sheared dolostones, and the dolostones adjacent to brecciated zone (Fig. 3a). Mn/Sr ratios stay low in the upper part of the section despite the elevated concentration of Mn. This is because the Sr concentration increases upward in the section at a higher rate as compared with Mn (Fig. 3a).

### 3.5. Carbon isotope composition

All dolostones including the de-dolomitised varieties and shear zones are enriched in $^{13}C$ throughout the section (Fig. 2), with overall $\delta^{13}C$ values ranging from +5·8 to +8·9‰ ($+7{\cdot}5 \pm 0{\cdot}6$‰, $n=95$). One sample obtained at depth 272·7 m from a 1-mm-thick, post-peak metamorphic, dolomite veinlet has $\delta^{13}C = -1{\cdot}4$‰.

Four separate $\delta^{13}C$ excursions have been identified in the succession, all showing a gradual upward decrease in $\delta^{13}C$, separated by relatively sharp, positive $\delta^{13}C$ offsets of the order of 0·5–1·5‰ (Fig. 2). Excursion 1 is not robust because of the scarcity of $\delta^{13}C$ data from siliciclastic-dominated units I–IV. However, the upward decrease in $\delta^{13}C$ from +8 to +7‰ coincides with the transition from interdistributary areas on the coastal plain to a shallow-water lacustrine facies. The 1·5‰ positive offset at the base of the following Excursion 2 is coincident with the switch to more restricted, ephemeral ponds on the distal braidplain (Melezhik & Fallick 2005). Excursion 2, with a gradual decrease in $\delta^{13}C$ from Unit V (+8·5‰) to the middle part of Unit VII (+7·5‰), and the positive offset in $\delta^{13}C$ above it, are not readily linked with any obvious changes in sedimentological features of the rocks. Excursion 3 shows rather erratic decrease from the middle of Unit VII (+8‰) towards the top of Unit IX (+7‰), although it is masked by several departures towards lower $\delta^{13}C$ values. The overall isotopic shift, similar to the previous case, cannot be linked with definite changes in sedimentological characteristics of the rocks. The third $\delta^{13}C$ offset of ~1‰, at the base of Excursion 4, is defined by a rapid switch in the depositional setting from a carbonate shoreline to a rift-bound playa-lake (Melezhik & Fallick 2005). Excursion 4 represents a prominent and rapid $\delta^{13}C$ decrease from +7·5‰ to +6·0‰ towards the upper contact of the succession within an interval of 50 m (Fig. 2).

The lowest $\delta^{13}C$ values have been measured from the lowermost and the uppermost parts of the section (Fig. 2). In the first case, they are associated with the quartzite-hosted lenses of de-dolomitised rocks within siliciclastic-dominated units I–IV (Fig. 3b), whereas, in the second case, $^{13}C$-depletion is related to the contact with the overlying volcanic rocks (Fig. 3b). The dolostones of mixed siliciclastic-dolostone Unit V and dolostone-dominated Unit VI are most enriched in $^{13}C$ ($\delta^{13}C = +8{\cdot}4$‰, on average). Despite the complexity in the stratigraphic variation of $\delta^{13}C$, the overall data show a more-or-less normal distribution (Fig. 5a), suggesting no obvious secondary alteration. Overall, $\delta^{13}C$ values exhibit very little dependence on sample position with respect to the brecciated and sheared zones (Fig. 3b).

### 3.6. Oxygen isotope composition

$\delta^{18}O$ fluctuates within a large range, i.e. 10·8–20·4‰, with an average value of $16{\cdot}8 \pm 2{\cdot}4$‰ ($n=95$). Although $\delta^{18}O$ exhibits a different trend with respect to $\delta^{13}C$, four separate excursions can be identified (Fig. 2). The first shows irregular fluctuations through Unit II. The second exhibits gradual increase from Unit V (11‰) through Unit VII (19‰). The third is characterised by a decrease from 20‰ to 14‰ towards the lower shear

https://doi.org/10.1017/S0263593300001152 Published online by Cambridge University Press

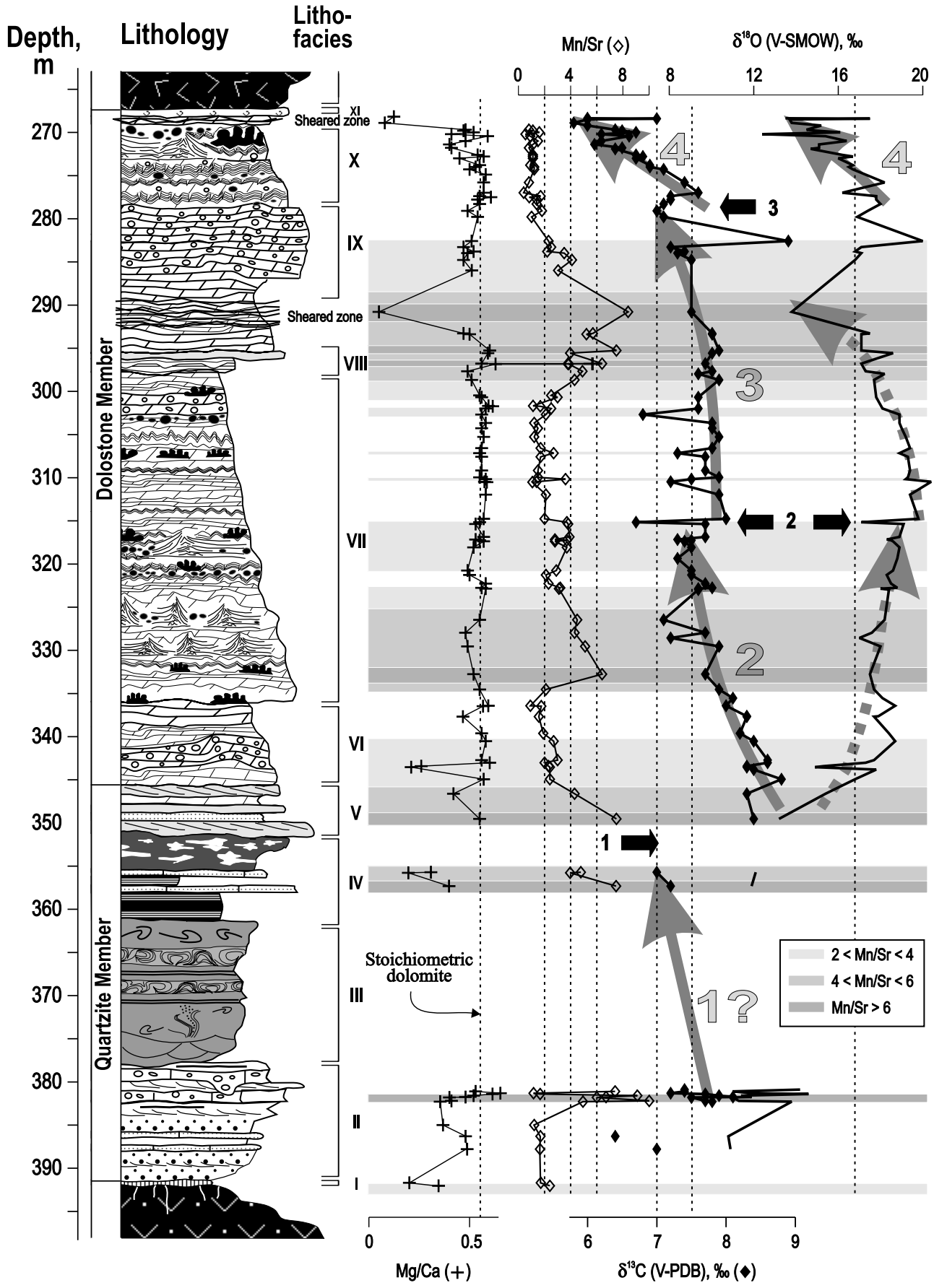


https://doi.org/10.1017/S0263593300001152 Published online by Cambridge University Press

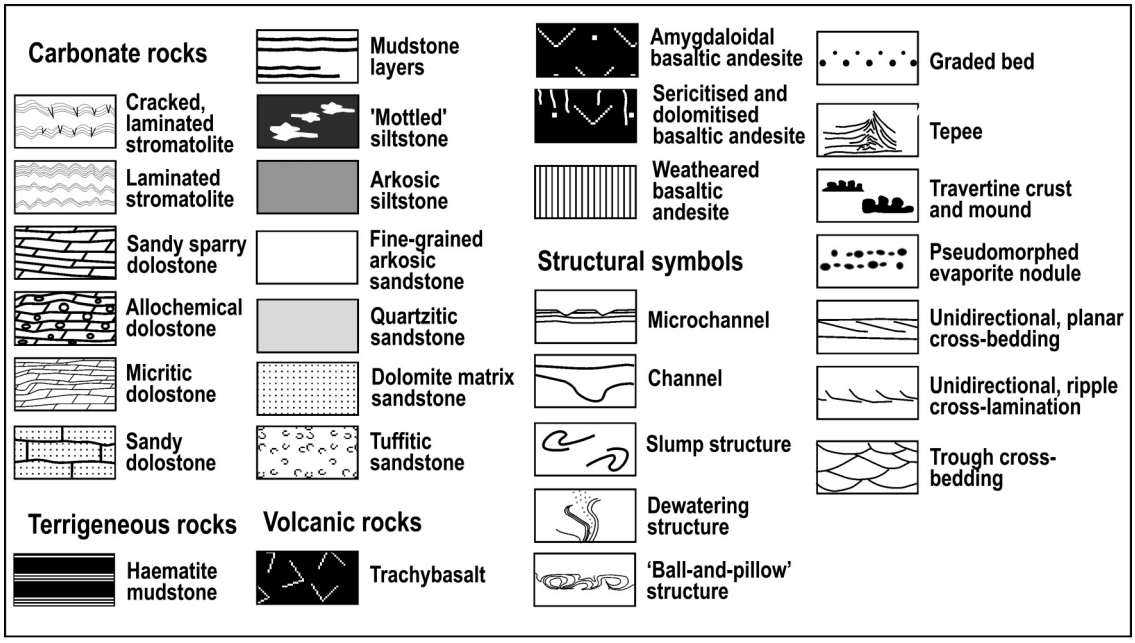


**Figure 2** Lithofacies versus Mg/Ca and Mn/Sr ratios, and carbon and oxygen isotopic composition of the carbonate rocks of the Kuetsjärvi Sedimentary Formation. Large, pale-grey numbers against arrowhead lines indicate short-term, stratigraphic variations of $\delta^{13}C$ and $\delta^{18}O$. The black arrows and numbers indicate sharp, positive, $\delta^{13}C$ and $\delta^{18}O$ offsets. See text for discussion.

zone (Figs 2 & 3b). Excursion 4 represents a prominent and rapid $\delta^{18}O$ decrease from 20‰ to 13‰ towards the upper contact of the succession within an interval of 50 m (Fig. 2).

A slight depletion in $^{18}O$ (16‰<$\delta^{18}O$<18·5‰) has been measured from Unit X dolostones, and from those located in or near the sheared zone (Fig. 3b). The lowermost $\delta^{18}O$ values (<16‰) are associated with the quartzite-hosted lenses of the de-dolomitised rocks within siliciclastic-dominated units I–IV, as well as with the upper part of the section (Fig. 3b). The main dolostone body shows a symmetrical, gradual $\delta^{18}O$ decrease from the centre (19·5‰) towards the brecciated and sheared zone with chlorite veinlets (17·0‰; Fig. 3b). When all $\delta^{18}O$ data are plotted against the carbonate concentrations ($C_{carb}$), the rocks with $\delta^{18}O$<16‰ and those with $\delta^{18}O$>16‰ are distributed along different regression lines (Fig. 4c). Although both subsets exhibit a positive $\delta^{18}O$–$C_{carb}$ correlation, the samples most depleted in $^{18}O$ are characterised by a stronger dependence of $\delta^{18}O$ on $C_{carb}$. Overall, $\delta^{18}O$ values reflect sample positions with respect to the brecciated, sheared zones and siliciclastic facies. The gradual $\delta^{18}O$ decrease in the upper part of the section is related to both the stratigraphy and the contact zone (Figs 2 & 3b) and it is coherent with the fourth excursion of $\delta^{13}C$. One sample obtained at depth 272·7 m from a 1-mm-thick, post-peak metamorphic, dolomite veinlet shows $\delta^{18}O$=6·6‰. A histogram for the overall data shows a $\delta^{18}O$ distribution skewed towards lower values (Fig. 5b), suggesting secondary alteration.

### 3.7. Carbon and oxygen isotopes versus Mn and Sr concentration and Mg/Ca and Mn/Sr ratios

The overall data show a weak positive correlation between $\delta^{13}C$ and $\delta^{18}O$ ($r$=+0·37, $n$=95). However, if the quartzite-hosted, de-dolomitised rocks are plotted separately from other dolostones, both subsets are characterised by a significant, positive correlation ($r$=0·53 and $r$=0·63, respectively; Fig. 4d). Interestingly, different intervals may show a negative $\delta^{13}C$-$\delta^{18}O$ correlation. The correlation is highly positive between 268·0 and 298·4 m ($r$=0·77, $n$=38, >99·9%; Fig. 4d, upper panel), whereas it is significantly negative between 315·1 and 346·4 m ($r$= − 0·52, $n$=29, >99·0%; Fig. 4d, lower panel). The first interval characterises units VII–XII, and the second Unit VI and the lower part of Unit VII (Fig. 2).

Mn/Sr ratios do not show a significant correlation with $\delta^{13}C$ (Fig. 4e). The overall data suggest a strong, negative Sr-$\delta^{13}C$ correlation ($r$= − 0·63, $n$=95, >99·9%; Fig. 4f). This is mainly driven by two subsets, namely by dolostones from the upper contact zone (274·0–268·0 m, $r$= − 0·43, $n$=20; Fig. 4f), and those hosted by siliciclastic-dominated units I–V from the lower part of the section ($r$= − 0·70, $n$=14; Fig. 4f). The rest of the data show no correlation ($r$= − 0·03, $n$=50; Fig. 4f).

The relationship between $\delta^{18}O$ values and Mn/Sr ratios is rather complex. The dolostones from different intervals plot on a $\delta^{18}O$-Mn/Sr diagram in different fields (Fig. 4g). The dolostone hosted by siliciclastic-dominated units I–VI with the lowest $\delta^{18}O$ values and highest Mn/Sr ratios shows no correlation between these two parameters. The dolostones from the upper contact zone show no correlation, whereas the dolostones from the brecciated and sheared zones show a positive correlation ($r$=0·56, $n$=17; Fig. 4g). The rest of the samples exhibit no correlation. A $\delta^{18}O$–Mg/Ca cross-plot displays a significant, positive correlation ($r$=0·44, $n$=91, >99·9%) if five de-dolomitised samples are excluded (Fig. 4h, inset). The $Al_2O_3$ concentration tends to correlate negatively with $\delta^{18}O$ (Fig. 4i).

### 3.8. Strontium isotope composition

Ten dolostone samples selected for Sr isotope analysis yielded $^{87}Sr/^{86}Sr$ ratios ranging from 0·70406 to 0·70623 (Table 2). The least radiogenic values (0·70406–0·70486) are measured from the uppermost part of the sequence. These samples contain up to 8 wt.% insoluble residue, mainly in the form of chlorite, talc and quartz. $^{87}Sr/^{86}Sr$ ratios show a significant negative correlation with the Sr concentration ($r$= − 0·89, >99·9%), and a significant positive correlation with $\delta^{18}O$ ($r$=0·86, 99·9%), $\delta^{13}C$ ($r$=0·83, >99·0%) and Mg/Ca ratios ($r$=0·78, >99%). The most radiogenic values (0·70560–0·70623) are measured from the

https://doi.org/10.1017/S0263593300001152 Published online by Cambridge University Press

**Table 1** Chemical and isotopic composition of the Kuetsjärvi Sedimentary Formation dolostones*

| Depth (m) | Sample description | Mg (%) | Ca (%) | Mn (ppm) | Sr (ppm) | Mg/Ca | Mn/Sr | $\delta^{13}C$ (‰) | $\delta^{18}O$ (‰) |
|---|---|---|---|---|---|---|---|---|---|
| Unit XI, mixed siliciclastic-dolostone: | | | | | | | | | |
| 268·0 | Calcitised DS | 2·75 | 13·4 | 652 | 574 | 0·21 | 1·14 | +5·9 | 13·7 |
| Shear zone carbonate rocks: | | | | | | | | | |
| 268·06 | Calcitised DS | n.d. | n.d. | n.d. | 618 | n.d. | n.d. | +6·0 | 13·5 |
| 268·1 | Calcitised DS | 9·65 | 26·8 | 847 | 981 | 0·36 | 0·86 | +7·0 | 17·5 |
| 268·2 | Calcitised DS | n.d. | n.d. | n.d. | 1069 | n.d. | n.d. | +6·0 | 13·7 |
| 268·6 | Calcitised DS | 1·90 | 24·0 | 771 | n.d. | 0·08 | n.d. | +5·8 | 13·8 |
| Unit X, dolostone-dominated: | | | | | | | | | |
| 268·9 | DM | n.d. | n.d. | n.d. | 555 | n.d. | n.d. | +6·0 | 15·2 |
| 269·4 | Calcitised DM | 10·9 | 22·7 | 539 | 651 | 0·48 | 0·80 | +6·4 | 14·5 |
| 269·5 | Calcitised DS | 9·91 | 21·2 | 616 | 543 | 0·47 | 1·10 | +6·5 | 15·0 |
| 269·7 | DS | 10·3 | 19·9 | 620 | 376 | 0·52 | 1·60 | +6·7 | 16·1 |
| 269·9 | DS | 9·22 | 18·5 | 293 | 441 | 0·50 | 0·66 | +6·2 | 12·4 |
| 270·2 | DM | 12·8 | 21·7 | 539 | 588 | 0·59 | 0·90 | +6·6 | 15·4 |
| 270·7 | Calcitised DM | 9·76 | 20·2 | 462 | 304 | 0·48 | 1·50 | +6·2 | 16·4 |
| 271·1 | Calcitised DM | 8·50 | 21·1 | 385 | 358 | 0·40 | 1·10 | +6·1 | 15·1 |
| 271·5 | Calcitised DS | 8·21 | 19·8 | 231 | 272 | 0·41 | 0·80 | +6·5 | 15·1 |
| 271·6 | MD | 11·6 | 22·3 | 424 | 514 | 0·52 | 0·82 | +6·4 | 14·7 |
| 272·3 | MD | 9·8 | 18·1 | 231 | 209 | 0·54 | 1·10 | +6·7 | 16·2 |
| 272·5 | DM | 10·7 | 18·9 | 234 | 211 | 0·57 | 1·10 | +6·8 | 16·7 |
| 272·7 | DS | 9·83 | 21·6 | 229 | 201 | 0·45 | 1·10 | +6·7 | 16·0 |
| 273·5 | DM | 9·98 | 18·2 | 150 | 168 | 0·55 | 0·90 | +6·9 | 16·7 |
| 273·7 | DM | 7·76 | 14·7 | 154 | 125 | 0·53 | 1·20 | +6·9 | 16·5 |
| 274·0 | DM | 8·17 | 16·4 | 149 | 130 | 0·50 | 1·20 | +7·1 | 16·7 |
| 275·5 | MD | 10·8 | 19·1 | 153 | 200 | 0·57 | 0·80 | +7·4 | 18·2 |
| 276·7 | DS | 10·7 | 18·8 | 77 | 178 | 0·57 | 0·40 | +7·6 | 16·2 |
| 277·1 | MD | 8·48 | 15·4 | 237 | 140 | 0·55 | 1·70 | +7·2 | 17·8 |
| 277·5 | MD | 9·32 | 17·3 | 230 | 166 | 0·54 | 1·40 | +7·2 | 17·8 |
| 278·0 | MD | 10·6 | 19·4 | 231 | 171 | 0·55 | 1·40 | +7·1 | 18·0 |
| Unit IX, dolostone-dominated: | | | | | | | | | |
| 278·8 | Calcitised DS | 8·20 | 16·6 | 225 | 132 | 0·49 | 1·80 | +7·0 | 17·4 |
| 279·5 | DS | 10·6 | 19·6 | 147 | 158 | 0·54 | 1·00 | +7·1 | 16·9 |
| 282·3 | DS | 7·70 | 15·1 | 234 | 102 | 0·51 | 2·30 | +8·9 | 20·0 |
| 283·0 | Calcitised DS | 7·27 | 15·5 | 231 | 93 | 0·47 | 2·50 | +7·2 | 17·1 |
| 283·5 | DS | 7·05 | 13·5 | 157 | 69 | 0·52 | 2·20 | +7·4 | 16·8 |
| 283·7 | Calcitised DS | 6·95 | 14·1 | 226 | 66 | 0·49 | 3·50 | +7·3 | 17·1 |
| 284·5 | Calcitised DS | 7·44 | 15·7 | 235 | 56 | 0·47 | 4·10 | +7·5 | 16·8 |
| Shear zone carbonate rocks: | | | | | | | | | |
| 290·5 | CM | 1·51 | 29·2 | 1078 | 128 | 0·05 | 8·40 | +7·5 | 13·8 |
| 293·0 | Calcitised DM | 8·86 | 18·6 | 462 | 81 | 0·47 | 5·70 | +7·8 | 17·5 |
| 293·1 | DM | 9·03 | 17·9 | 385 | 74 | 0·50 | 5·20 | +7·8 | 17·1 |
| 295·0 | DS | 8·74 | 14·4 | 616 | 82 | 0·60 | 7·50 | +7·9 | 17·1 |
| 295·3 | DS | 8·65 | 14·6 | 356 | 90 | 0·59 | 3·95 | +7·8 | 18·6 |
| Unit VIII, mixed siliciclastic-dolostone: | | | | | | | | | |
| 296·5 | CD | 8·14 | 14·5 | 620 | 96 | 0·56 | 6·40 | +7·7 | 17·1 |
| 297·4 | Calcitised CD | 6·78 | 13·8 | 462 | 94 | 0·49 | 4·90 | +7·8 | 17·3 |
| 297·7 | DM | 10·2 | 17·1 | 470 | 114 | 0·60 | 4·12 | +7·6 | 18·2 |
| Unit VII, dolostone-dominated: | | | | | | | | | |
| 298·4 | DM | 10·5 | 20·4 | 539 | 126 | 0·51 | 4·30 | +7·9 | 17·7 |
| 300·4 | MD | 10·3 | 18·6 | 231 | 78 | 0·56 | 3·00 | +7·6 | 17·8 |
| 301·7 | MD | 10·0 | 17·3 | 233 | 91 | 0·58 | 2·50 | +7·6 | 18·1 |
| 302·4 | MD | 11·3 | 20·2 | 241 | 109 | 0·56 | 2·10 | +6·8 | 18·9 |
| 303·4 | DM | 11·2 | 19·5 | 155 | 124 | 0·58 | 1·20 | +7·8 | 18·9 |
| 304·0 | MD | 10·3 | 18·3 | 162 | 103 | 0·56 | 1·50 | +7·8 | 19·0 |
| 305·0 | MD | 12·5 | 22·1 | 158 | 124 | 0·57 | 1·20 | +7·9 | 19·2 |
| 306·3 | MD | 12·1 | 21·7 | 154 | 92 | 0·56 | 1·70 | +7·8 | 19·4 |
| 306·9 | MD | 11·8 | 21·6 | 231 | 85 | 0·55 | 2·70 | +7·3 | 18·9 |
| 307·3 | MD | 12·6 | 22·6 | 146 | 92 | 0·56 | 1·70 | +7·7 | 19·3 |
| 308·9 | DS | 11·5 | 20·4 | 154 | 101 | 0·56 | 1·50 | +7·7 | 19·4 |
| 309·7 | MD | 10·3 | 18·6 | 158 | 106 | 0·55 | 1·50 | +7·9 | 19·3 |
| 309·9 | DM | 9·52 | 16·4 | 308 | 85 | 0·58 | 3·60 | +7·5 | 19·2 |

https://doi.org/10.1017/S0263593300001152 Published online by Cambridge University Press

**Table 1** *Continued*

| Depth (m) | Sample description | Mg (%) | Ca (%) | Mn (ppm) | Sr (ppm) | Mg/Ca | Mn/Sr | $\delta^{13}C$ (‰) | $\delta^{18}O$ (‰) |
|---|---|---|---|---|---|---|---|---|---|
| 310·2 | DM | 10·7 | 18·6 | 119 | 86 | 0·57 | 1·38 | +7·2 | 20·4 |
| 311·7 | MD | 10·3 | 18·0 | 159 | 75 | 0·58 | 2·10 | +7·9 | 19·4 |
| 314·5 | MD | 13·0 | 22·9 | 147 | 76 | 0·57 | 2·00 | +8·0 | 19·8 |
| 314·9 | DM | 9·28 | 16·9 | 230 | 62 | 0·55 | 3·70 | +6·7 | 17·1 |
| 315·1 | DM | 8·57 | 16·3 | 231 | 61 | 0·53 | 3·80 | +7·7 | 19·1 |
| 316·6 | DS and DM | 10·2 | 17·8 | 237 | 59 | 0·57 | 3·90 | +7·7 | 18·9 |
| 316·9 | DS and DM | 8·42 | 15·9 | 154 | 55 | 0·53 | 2·80 | +7·3 | 18·3 |
| 317·0 | DM | 9·62 | 17·5 | 227 | 63 | 0·55 | 3·70 | +7·5 | 18·5 |
| 317·1 | MD | 12·9 | 22·6 | 241 | 83 | 0·57 | 2·80 | +7·4 | 18·6 |
| 317·8 | DM | 10·2 | 19·7 | 230 | 62 | 0·52 | 3·70 | +7·5 | 18·9 |
| 319·1 | MD | n.d. | n.d. | n.d. | 70 | n.d. | n.d. | +7·3 | 18·8 |
| 320·5 | Calcitised MD | 11·4 | 23·1 | 231 | 79 | 0·49 | 2·90 | +7·5 | 18·6 |
| 321·0 | DM | 10·2 | 20·5 | 140 | 73 | 0·50 | 2·10 | +7·5 | 18·3 |
| 322·0 | DM | 10·1 | 17·5 | 154 | 68 | 0·58 | 2·30 | +7·7 | 18·5 |
| Unit VII, dolostone-dominated: | | | | | | | | | |
| 322·5 | MD | 12·9 | 23·3 | 242 | 72 | 0·56 | 3·20 | +7·8 | 18·8 |
| 322·6 | MD | 13·4 | 23·1 | 234 | 75 | 0·58 | 3·10 | +7·6 | 18·0 |
| 322·7 | DM | 13·7 | 21·2 | 139 | 80 | 0·65 | 1·73 | +7·6 | 18·4 |
| 326·2 | DM | 9·53 | 17·3 | 230 | 51 | 0·55 | 4·50 | +7·1 | 18·2 |
| 327·7 | Calcitised DM | 10·0 | 20·8 | 308 | 72 | 0·48 | 4·30 | +7·7 | 17·6 |
| 328·3 | DM | n.d. | n.d. | n.d. | n.d. | n.d. | n.d. | +7·2 | 17·0 |
| 329·3 | Calcitised DM | 9·3 | 19·2 | 395 | 75 | 0·49 | 5·10 | +7·9 | 18·0 |
| 332·5 | DM | 10·9 | 21·1 | 379 | 60 | 0·52 | 6·40 | +7·7 | 17·5 |
| 334·3 | DM | 10·0 | 18·4 | 154 | 75 | 0·55 | 2·10 | +7·9 | 17·7 |
| 335·3 | MD | 12·0 | 19·9 | 100 | 88 | 0·60 | 1·14 | +8·1 | 18·1 |
| Unit VI, dolostone-dominated: | | | | | | | | | |
| 336·2 | DS | 8·72 | 14·7 | 59 | 65 | 0·59 | 0·91 | +8·0 | 18·7 |
| 337·4 | Calcitised DS | 9·09 | 19·3 | 246 | 105 | 0·47 | 2·35 | +8·3 | 17·9 |
| 337·46 | DS | n.d. | n.d. | n.d. | n.d. | n.d. | n.d. | +8·3 | 17·7 |
| 339·4 | MD | 12·8 | 22·9 | 155 | 79 | 0·56 | 1·90 | +8·2 | 18·4 |
| 340·3 | MD | 12·9 | 22·1 | 243 | 85 | 0·58 | 2·70 | +8·4 | 18·7 |
| 342·5 | DS | 10·1 | 18·2 | 308 | 102 | 0·56 | 3·00 | +8·6 | 17·7 |
| 342·8 | DM | 13·5 | 22·7 | 235 | 113 | 0·60 | 2·00 | +8·6 | 17·3 |
| 343·2 | Calcitised DS | 6·73 | 26·3 | 385 | 166 | 0·26 | 2·30 | +8·3 | 15·3 |
| 343·3 | Calcitised DS | 5·81 | 27·0 | 391 | 161 | 0·21 | 2·40 | +8·3 | 14·9 |
| 343·6 | Calcitised DS | 6·52 | 17·4 | 185 | 130 | 0·37 | 1·42 | +8·4 | 17·8 |
| 344·7 | DM | 8·79 | 15·3 | 234 | 98 | 0·57 | 2·40 | +8·8 | 16·8 |
| Unit V, mixed siliciclastic-dolostone: | | | | | | | | | |
| 346·4 | Calcitised DS | 8·16 | 19·2 | 462 | 108 | 0·42 | 4·30 | +8·3 | 15·4 |
| 349·3 | DM | 11·8 | 21·2 | 1155 | 155 | 0·55 | 7·50 | +8·4 | 13·2 |
| Unit IV, mixed siliciclastic-dolostone: | | | | | | | | | |
| 355·5 | DS | n.d. | n.d. | n.d. | n.d. | n.d. | n.d. | +7·0 | 12·1 |
| 357·1 | Calcitised DS | 7·62 | 19·1 | 1838 | 246 | 0·40 | 7·47 | +7·2 | 11·9 |
| Unit II, mixed siliciclastic-dolostone: | | | | | | | | | |
| 380·7 | CD | n.d. | n.d. | n.d. | 114 | n.d. | n.d. | +7·4 | 14·2 |
| 380·9 | DM | 9·72 | 18·1 | 1001 | 135 | 0·53 | 7·40 | +7·4 | 11·0 |
| 381·1 | CD | 8·33 | 12·7 | 119 | 103 | 0·65 | 1·15 | +7·2 | 11·9 |
| 381·2 | DM | 7·16 | 11·6 | 178 | 107 | 0·61 | 1·66 | +7·7 | 14·6 |
| 381·4 | DM | 8·63 | 16·5 | 1078 | 118 | 0·52 | 9·10 | +7·9 | 11·4 |
| 381·6 | Calcitised DM | 8·35 | 17·3 | 924 | 138 | 0·48 | 6·70 | +8·1 | 11·9 |
| Unit II, mixed siliciclastic-dolostone: | | | | | | | | | |
| 381·65 | Calcitised DM | 7·23 | 18·1 | 847 | 142 | 0·40 | 6·00 | +7·5 | 11·0 |
| 382·0 | Calcitised DM | 7·57 | 18·3 | 1309 | 131 | 0·41 | 10·00 | +7·7 | 11·3 |
| 382·1 | Calcitised DM | 6·37 | 18·0 | 593 | 120 | 0·35 | 4·94 | +7·8 | 13·8 |
| 386·1 | Calcitised CD | 7·88 | 16·4 | 474 | 281 | 0·48 | 1·69 | +6·4 | 10·8 |
| 387·6 | Calcitised CD | 8·66 | 17·7 | 481 | 287 | 0·49 | 1·65 | +7·0 | 10·9 |

*Abbreviations: (CD) crystalline dolostone; (CM) micritic calcite; (DM) dolomicrite; (MD) microbial dolomite; (DS) dolosparite; and (n.d.) not determined.

https://doi.org/10.1017/S0263593300001152 Published online by Cambridge University Press

**Table 2** Geochemical, C-O and Rb-Sr isotope data for the Kuetsjärvi Sedimentary Formation dolostones

| Sample number | Ca (%) | Mg (%) | Mn (ppm) | Fe (ppm) | Rb* (ppm) | Sr* (ppm) | Mg/Ca | Mn/Sr | $\delta^{13}C$† (‰) | $\delta^{18}O$† (ppm) | $^{87}Rb/^{86}Sr$ | $^{87}Sr/^{86}Sr$ (measured) | $^{87}Sr/^{86}Sr$ (initial) |
|---|---|---|---|---|---|---|---|---|---|---|---|---|---|
| *Pale pink and brown micritic dolostone, partially calcitised dolostones and limestone* | | | | | | | | | | | | | |
| 268·1 | 26·8 | 9·65 | 847 | | 0·78 | 1750 | 0·36 | 0·9 | +7·0 | 17·5 | 0·0013 | 0·70435 | 0·70431 |
| 268·2 | | | | | 0·12 | 1555 | | | +6·0 | 13·7 | 0·0002 | 0·70408 | 0·70407 |
| 269·4a | 23·6 | 6·90 | 488 | 555 | 0·26 | 750 | 0·29 | 0·7 | +6·4 | 14·5 | 0·0010 | 0·70459 | 0·70456 |
| | | | | | | | | | **+6·8** | **16·7** | | | |
| | | | | | | | | | *+5·6* | *12·2* | | | |
| 269·4c | 21·8 | 8·61 | 393 | 658 | 0·10 | 745 | 0·39 | 0·5 | n.d. | n.d. | 0·0004 | 0·70407 | 0·70406 |
| | | | | | | | | | **+7·1** | **16·4** | | | |
| | | | | | | | | | *+6·6* | *14·2* | | | |
| 271·6a | 32·0 | 0·70 | 483 | 183 | 0·45 | 550 | 0·02 | 0·9 | n.d. | n.d. | 0·0024 | 0·70417 | 0·70410 |
| | | | | | | | | | **+7·2** | **18·4** | | | |
| | | | | | | | | | *+6·5* | *12·5* | | | |
| 271·6c | 27·2 | 4·05 | 401 | 290 | 0·10 | 345 | 0·15 | 1·2 | n.d. | n.d. | 0·0008 | 0·70414 | 0·70412 |
| | | | | | | | | | **+6·4** | **18·1** | | | |
| | | | | | | | | | *+6·3* | *13·4* | | | |
| 272·7a | 20·9 | 12·3 | 81 | 627 | 0·14 | 285 | 0·59 | 0·3 | n.d. | n.d. | 0·0014 | 0·70490 | 0·70486 |
| | | | | | | | | | **+5·5** | **18·3** | | | |
| | | | | | | | | | *+5·9* | *16·7* | | | |
| *Sparry dolostones* | | | | | | | | | | | | | |
| 307·3 | 21·6 | 13·2 | 82 | 460 | 0·33 | 91 | 0·61 | 0·9 | +7·7 | 19·4 | 0·0107 | 0·70653 | 0·70620 |
| 314·5 | 22·9 | 13·1 | 70 | 512 | 0·23 | 79 | 0·57 | 0·9 | +8·0 | 19·8 | 0·0075 | 0·70645 | 0·70623 |
| 322·5 | 23·3 | 12·9 | 120 | 665 | 0·08 | 71 | 0·55 | 1·7 | +7·8 | 18·8 | 0·0032 | 0·70585 | 0·70575 |
| 322·6 | 22·1 | 12·8 | 132 | 700 | 0·10 | 72 | 0·58 | 1·8 | +7·6 | 18·0 | 0·0040 | 0·70592 | 0·70579 |
| 339·4 | 23·0 | 12·8 | 86 | 575 | 0·16 | 82 | 0·56 | 1·0 | +8·2 | 18·4 | 0·0056 | 0·70595 | 0·70578 |
| 340·3 | 21·5 | 12·9 | 124 | 610 | 0·34 | 91 | 0·60 | 1·4 | +8·4 | 18·6 | 0·0108 | 0·70592 | 0·70560 |
| *Micritic dolostone* | | | | | | | | | | | | | |
| 342·8 | 21·6 | 13·2 | 150 | 806 | 0·41 | 111 | 0·61 | 1·4 | +8·6 | 17·3 | 0·0107 | 0·70655 | 0·70622 |
| *Post-kinematic calcite veinlet* | | | | | | | | | | | | | |
| 272·7f | 32·7 | 0·47 | 292 | 119 | 0·27 | 155 | 0·01 | 1·9 | −1·4 | 6·6 | 0·0051 | 0·72981 | 0·72966 |
| *Travertine dolomite* | | | | | | | | | | | | | |
| 16‡ | n.d. | n.d. | n.d. | n.d. | 0·78 | 56+10 | n.d. | n.d. | +5·8 | 20·4 | | 0·7063 | |
| 15‡ | 45·5 | 20·6 | n.d. | n.d. | 1·04 | 20+8 | 0·45 | n.d. | +5·1 | 19·9 | | 0·7064 | |
| 13‡ | 45·6 | 21·4 | n.d. | n.d. | 5·5 | 96+10 | 0·47 | n.d. | +2·4 | 17·6 | | 0·7057 | |
| 11‡ | 45·4 | 21·0 | n.d. | n.d. | 0·64 | 45+20 | 0·46 | n.d. | −0·3 | 15·8 | | 0·7073 | |
| 8‡ | 46·1 | 20·9 | n.d. | n.d. | 1·06 | 15+7 | 0·45 | n.d. | −5·3 | 13·3 | | 0·7067 | |

*Rb and Sr contents were determined by standard isotope dilution and solid-source mass spectrometry.
†$\delta^{13}C$ and $\delta^{18}O$ data shown in bold-letters are obtained by sequential analysis of dolomite; $\delta^{13}C$ and $\delta^{18}O$ data shown in italic are obtained by sequential analysis of calcite; and (n.d.) not determined. ‡Ca, Mg, $\delta^{13}C$ and $\delta^{18}O$ data are from Melezhik & Fallick (2001).

middle and lower parts of the Dolostone Member (Fig. 2). The analysed samples are devoid of quartz, feldspar and mica ($SiO_2$=0–1·6 wt.%; $Al_2O_3$=0–0·08 wt.%).

Five sub-milligram, micro-cored samples of the individual travertine laminae from the upper part of the sequence yielded $^{87}Sr/^{86}Sr$ ratios ranging from 0·7057 to 0·7067 (Table 2), although with a significant analytical error caused by small sample weights (1·9 to 2·6 mg) and low Sr concentrations (Table 2).

A late, post-peak metamorphic calcite vein is marked by highly radiogenic strontium value of 0·72966 (Table 2).

## 4. Post-depositional alteration and inferred resetting in carbon and oxygen isotope systems

The KSF dolostones underwent diagenesis, metamorphism and concomitant deformation during the c. 1850 Ma Svecofennian orogeny. Thus, the preservation of primary sedimentary isotope composition may be questioned because, during a long post-depositional history, diagenesis, deep burial and metamorphism had ample opportunity to alter the original isotope ratios.

### 4.1. Diagenetic and catagenetic alterations

The mineralogical and geochemical expression of diagentic alterations of the KSF rocks remains poorly understood. Apart from diagenetic alteration, the KSF rocks were subject to catagenetic alteration caused by horizontal and vertical infiltration of $H_2S$-free reducing fluids (Melezhik 1992). The catagenetic alteration resulted in bleaching and discoloration of 'red beds', accompanied by reduction of $Fe^{3+}$ to $Fe^{2+}$ and depletion in $Fe_{tot}$ concentration (Melezhik 1992).

### 4.2. Regional metamorphism

The rocks experienced three episodes of deformation ($D_1$, $D_2$ and $D_3$), culminating in amphibolite facies metamorphism. However, the metamorphic facies show a clear zoning (Petrov & Voloshina 1995). In the central Pechenga Zone, at the present-day erosional surface, the KSF underwent biotite–actinolite metamorphism, which gradually passes into

https://doi.org/10.1017/S0263593300001152 Published online by Cambridge University Press

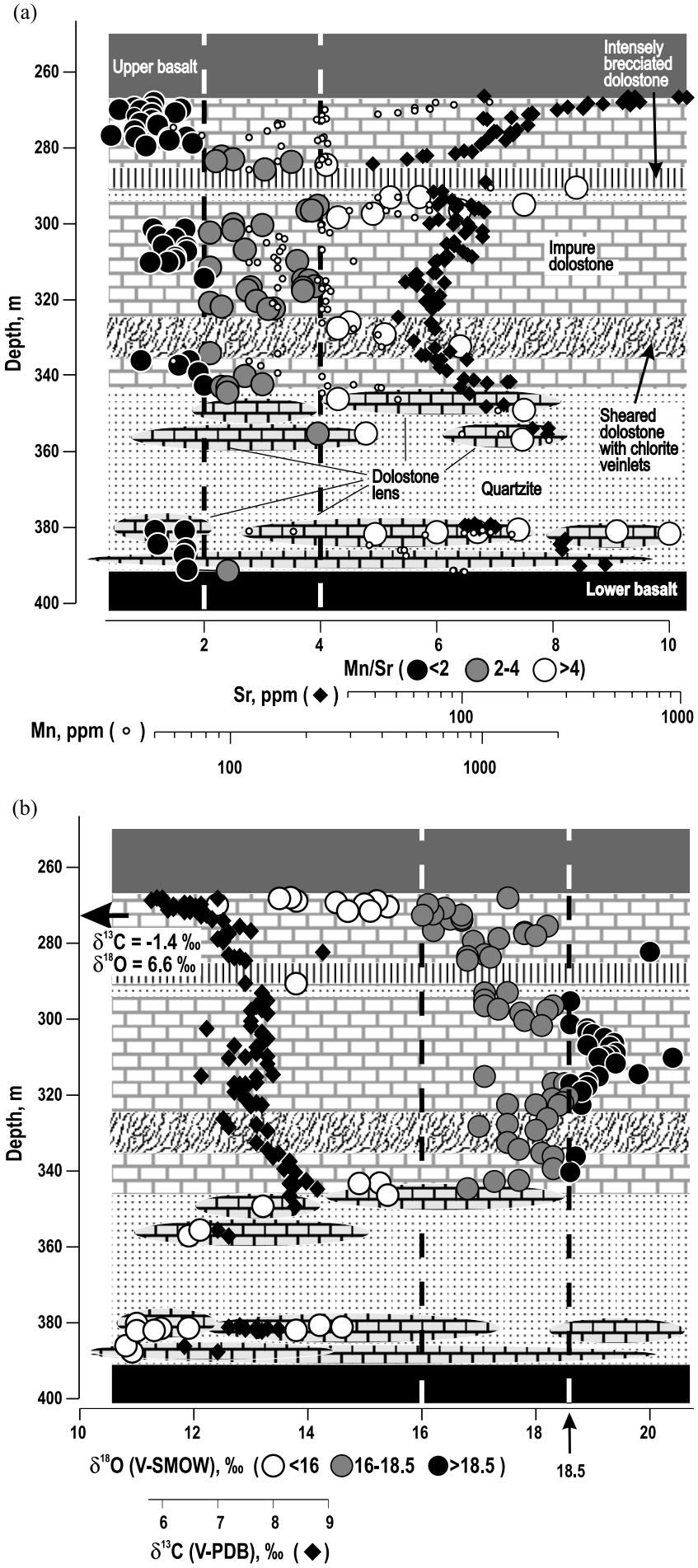


**Figure 3** (a) Mn/Sr ratio and Sr, Mn concentrations and (b) carbon and oxygen isotopic composition versus main geological features of the Kuetsjärvi Sedimentary Formation. The geological section is modified after Melezhik *et al.* 2003. The arrow in (b) indicates the position and isotopic values of 1-mm-thick dolomite veinlets formed during retrograde metamorphism.

https://doi.org/10.1017/S0263593300001152 Published online by Cambridge University Press

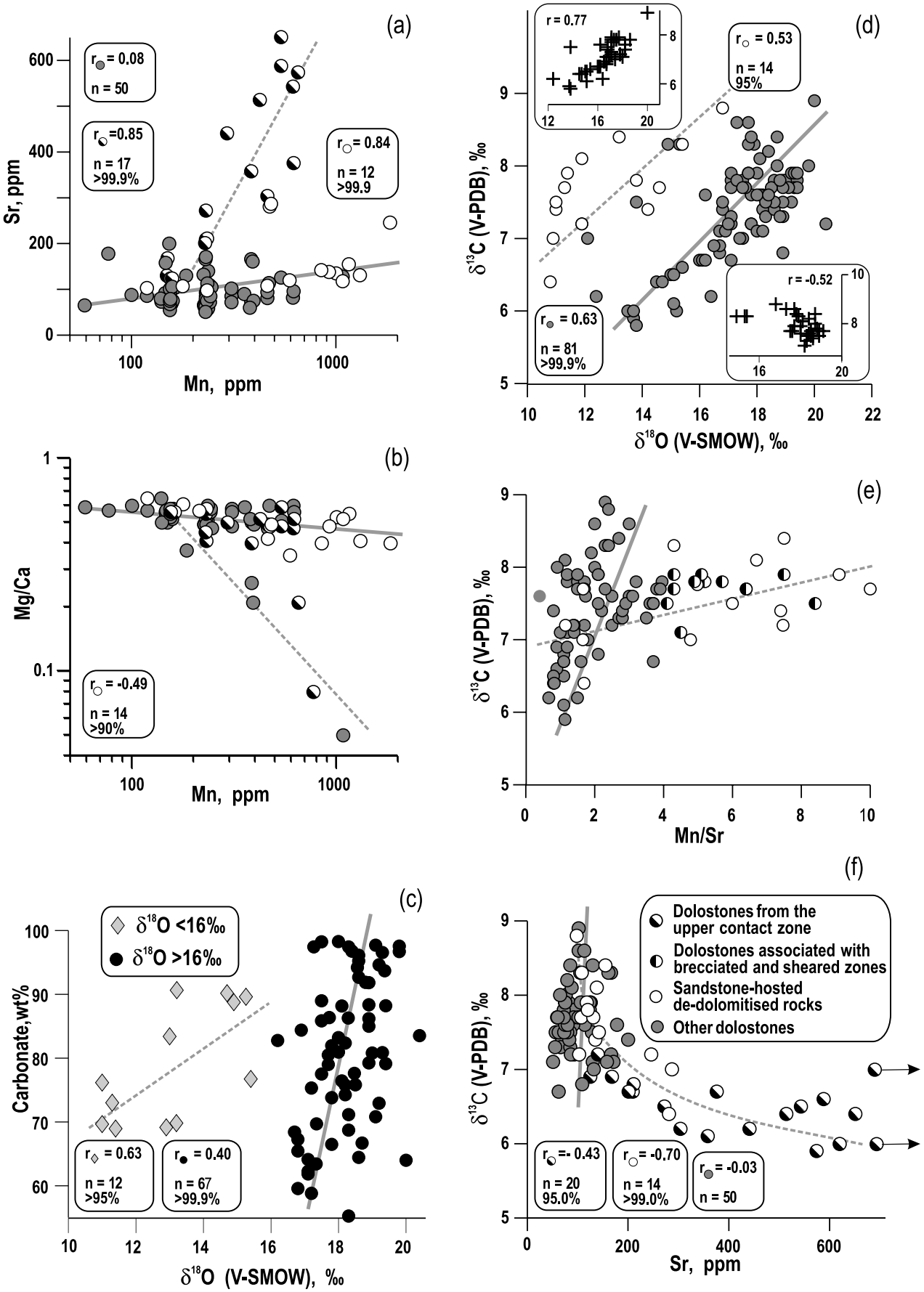


**Figure 4** (a)–(f).

epidote–amphibolite facies towards the western and eastern flanks of the zone (Melezhik *et al.* 2003). The succession intersected by DHX, from which all the samples for isotopic study have been collected, is entirely situated within the biotite–actinolite metamorphic facies. Primary mineral parageneses of the KSF dolostones are represented by

https://doi.org/10.1017/S0263593300001152 Published online by Cambridge University Press

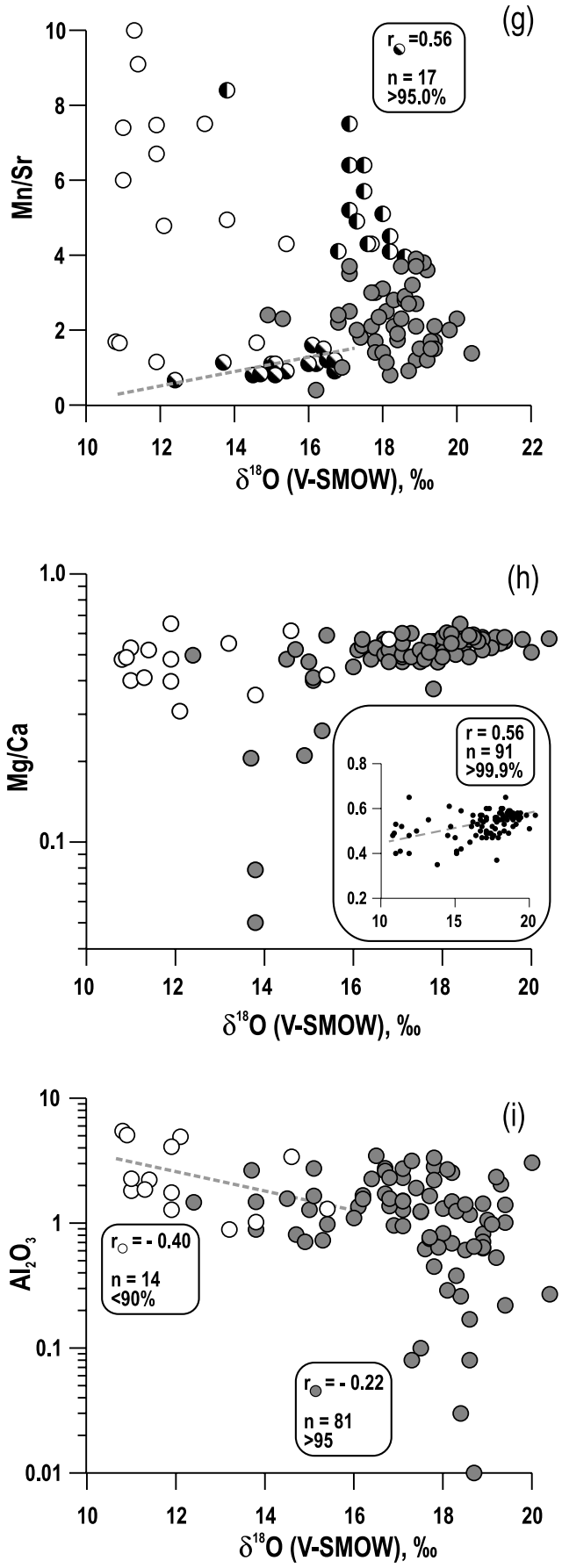


**Figure 4** (g)–(i).

**Figure 4** Discrimination diagrams for Kuetsjärvi Sedimentary Formation dolostones. Major correlation trends are indicated by lines. In (d), the upper inset illustrates a highly positive $\delta^{13}C$–$\delta^{18}O$ correlation ($r$=0·77, $n$=38, >99·9%) for the dolostones located between 268·0 and 298·4 m, whereas the lower inset shows a significant negative correlation ($r$= − 0·52, $n$=29, >99·0%) for the dolostones developed between 315·1 and 346·4 m. The inset in (h) is a Mg/Ca versus $\delta^{18}O$ cross-plot in linear scale illustrating a significant positive correlation for the major subset of the data.

https://doi.org/10.1017/S0263593300001152 Published online by Cambridge University Press

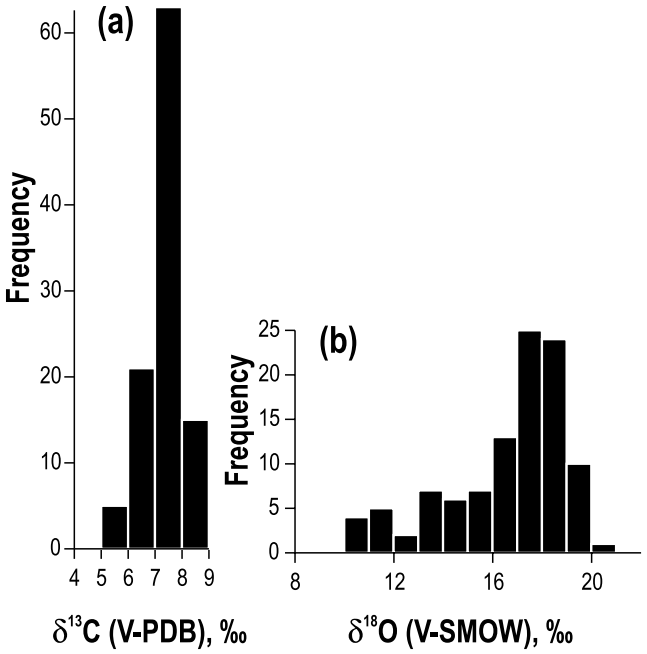


**Figure 5** (a) $\delta^{13}C$ and (b) $\delta^{18}O$ histograms for the Kuetsjärvi Sedimentary Formation dolostones.

dolomite + quartz + sericite ± K-feldspar ± calcite. The metamorphic parageneses in the biotite–actinolite facies are defined by the reaction: 3 dolomite + 4 quartz + 1 $H_2O \rightarrow$ 1 talc + 3 calcite$_2$ + 3 $CO_2$ (e.g. Winkler 1979). Drill hole X intersected partially sheared and brecciated rocks within a narrow NW–SE trending block bounded by faults which are connected to one of the major fault zones, the Luchlompolo Thrust (for details see Melezhik *et al.* 2003). The thrust defines a relatively permeable zone. The $D_3$ shearing and brecciation documented in several intervals is accompanied by sporadic development of low-temperature chlorite and quartz-chlorite veinlets which post-date the peak-metamorphism.

### 4.3. Resetting of the carbon isotope system

Several reversals of the $\delta^{13}C$–$\delta^{18}O$ correlations (Fig. 4d) documented throughout the succession (Fig. 3b) suggest that the fate of these two isotope systems were partially decoupled during the course of post-depositional history. Support for partial decoupling is provided by the fact that the $^{18}O$-depleted dolostones from the brecciated and sheared zones do not exhibit a sizeable depletion in $^{13}C$ (Fig. 3b). Moreover, the $\delta^{13}C$ histogram (Fig. 5a) does not suggest post-depositional isotopic resetting. However, one may argue that the positive $\delta^{13}C$–$\delta^{18}O$ correlation in two major subsets (Fig. 4d) might have been caused by partial re-equilibration of both the O and C isotopic systems. Nevertheless, this is not supported by a focused isotopic study (Melezhik *et al.* 2003; Melezhik & Fallick 2003) based on microcored samples of different carbonate phases which showed that, in the low-grade greenschist facies conditions, distinct textural components from the same parental dolostones collected from DHX yielded $\delta^{13}C$ values clustering within 1‰. There are no statistical differences between early dolomicrite, and late void- and fenestra-filling dolospar (Melezhik & Fallick 2003). However, genetically different dolomites retain their primary carbon isotopic characteristics. This is in contrast with $\delta^{18}O$ values, which show up to a 6‰ range associated with diagenetic/metamorphic resetting (Melezhik *et al.* 2003; Melezhik & Fallick 2003). However, isotopic composition of the dolomite veinlet suggests that very low $\delta^{13}C$ ($-1{\cdot}4$‰) and $\delta^{18}O$ (6·6‰) fluids were available during the post-peak metamorphic stage.

Brand & Veizer (1980) and Derry *et al.* (1992) reported that Mn and Sr can serve as a tool for calibration of the relative diagenetic rank of sequences. An increasing degree of post-depositional alteration leads to Sr depletion and Mn enrichment. Following Kaufman & Knoll (1995), one may assume that all the dolostones with Mn/Sr ratios exceeding 6·0 were affected by a post-sedimentary alteration. Surprisingly, the KSF dolostones show a tendency for positive correlation between Mn/Sr ratios and $\delta^{13}C$ values (Fig. 4e), which is exactly opposite to the predicted alteration trend (e.g. Brand & Veizer 1980; Derry *et al.* 1992; Kaufman & Knoll 1995). Moreover, there are no statistical differences in $\delta^{13}C$ between the samples with Mn/Sr>6 and those characterised by lower Mn/Sr ratios.

Two outstanding intervals showing $^{13}C$ depletion well below the average $\delta^{13}C$ value of $+7{\cdot}5 \pm 0{\cdot}6$‰ are located in the lower and particularly in the upper part of the succession. A partial isotopic repartitioning may not be ruled out for the lower-zone samples since they are all from thin lenses within permeable quartzites marked by Mn/Sr>4–6. However, it does not seem that the simple alteration scenario can also be invoked for the explanation of the upward, smooth, $\delta^{13}C$ decrease from +7·5‰ to +6·0‰ in the upper part of the succession. This is because different carbonate phases from the same parental dolostones collected from the upper part of the succession show $\delta^{13}C$ values clustering within 1‰ (Melezhik & Fallick 2003). It seems that very low $\delta^{13}C$ ($-1{\cdot}4$‰) and $\delta^{18}O$ (6·6‰) post-peak metamorphic fluids affected only those lithologies which were subject to deformation, brecciation and subsequent recrystallisation. Thus, both the trend and the actual $\delta^{13}C$ values may be considered to represent a close proxy to the primary composition of ambient water.

As has been stated earlier, the overall $\delta^{13}C$-curve is subdivided into four excursions which are separated by three relatively sharp, positive, $\delta^{13}C$ offsets (Fig. 2). These excursions and the offsets have apparently different origin. Excursion 1 and the 1·2‰ offset above it are apparently of a post-depositional origin caused by diagenetic overprint of the de-dolomitised rocks in the siliciclastic-dominated units I–IV. However, excursions 2, 3 and 4, with the two offsets in between are not associated with any obvious alteration features and may represent original depositional trends.

### 4.4. Resetting of the oxygen isotope system

Consideration of $\delta^{18}O$ and trace element distribution patterns clearly suggests post-depositional resetting trends which are accompanied by essentially invariant $\delta^{13}C$. It is not surprising that, in the course of post-depositional recrystallisation of carbonate phases, the $\delta^{13}C$ would be buffered by the dissolving precursor, while the $\delta^{18}O$, Mn and Sr would be partially shifted towards equilibrium with the ambient diagenetic fluids, because the sediment/water ratios of diagenetic systems (cf. Banner & Hanson 1990) are about $10^1$ : $10^2$–$10^3$:$10^4$ for oxygen, trace elements and carbon, respectively (cf. Land 1992).

In their previous work, the present authors have reported 5–11‰ depletion of the KSF dolostones in $^{18}O$, which took place in the transition from the biotite–actinolite to the epidote–amphibolite facies as a result of the decarbonation reaction coupled with isotopic exchange between the carbonates and fluids with an external source of oxygen (Melezhik *et al.* 2003). It was also shown that the biotite–actinolite facies dolostones from DHX are depleted in $^{18}O$ by 4‰ on average, as compared to the dolostones of a similar metamorphic facies, although sampled from the surface (Melezhik *et al.* 2003). This was assigned to oxygen isotope exchange of the dolomite with

https://doi.org/10.1017/S0263593300001152 Published online by Cambridge University Press

the external fluids which migrated through sheared and brecciated zones during the course of retrograde, post-peak metamorphic processes (Melezhik *et al.* 2003). Although this scenario is in general agreement with the more detailed current study, several reversals of the $\delta^{13}C$–$\delta^{18}O$ correlations documented throughout the succession (Fig. 4d) indicate more complex overall alteration pattern.

The composition of brecciated dolostones and those from the retrograde sheared zones suggests that post-peak metamorphic fluids responsible for the overall downward-shifting of $\delta^{18}O$ were relatively rich in Mn and relatively poor in Sr, thus resulting in the negative $\delta^{18}O$–Mn/Sr correlation (Fig. 4g) and Mn/Sr>4 (Fig. 3a). However, the most severe depletion in $^{18}O$ is documented in the quartzite-hosted lenses of quartz-rich, partially de-dolomitised dolostones. The Mg/Ca–$\delta^{18}O$ cross-plot shows no link between de-dolomitisation and depletion in $^{18}O$, and suggests that these two processes were decoupled.

Some of these quartzite-hosted dolostones have elevated Mn/Sr ratios, whereas others do not, which may indicate that post-depositional repartitioning of oxygen isotopes was caused by more than one fluid. The quartzite-hosted dolostones with higher Mn/Sr ratios were probably affected by a fluid of similar composition to the one which altered the brecciated and sheared dolostones (Fig. 3a). The others, with lower Mn/Sr ratios, show close similarity with the $^{18}O$-depleted dolostones from the upper contact zone. Both might have exchanged oxygen isotopes with a fluid infiltrating along the contact zones. The positive $\delta^{18}O$–Mn/Sr correlation (Fig. 4g) suggests that this fluid was rich in Mn. However, these geochemical features are difficult to reconcile with the proposition that the upper contact zone Sr-rich dolostones represent only a more altered equivalent of other dolostones. Alternatively, the Sr dichotomy documented in the succession may be a consequence of differences in the original mineralogy or chemistry of the precursors, whereas the varied degree of $^{18}O$ depletion was a consequence of differences in the nature of altering fluids. A polyphase alteration and multiple fluid sources are consistent with several regression trends revealed by various discrimination diagrams (Fig. 4). However, the smooth, upward $\delta^{18}O$ decrease in the upper part of the succession may still represent the original depositional trend, whereas initial, absolute $\delta^{18}O$ values were essentially altered and cannot be reconstructed. This is supported by the fact that $\delta^{18}O$ correlates positively with the largely preserved initial $\delta^{13}C$ values (Fig. 4d).

The positive correlation and significantly different $\delta^{18}O$–$C_{carb}$ gradients observed for the lower $\delta^{18}O$ ($r=0{\cdot}63$, mainly quartzite-hosted dolostones) and higher $\delta^{18}O$ ($r=0{\cdot}40$) subsets (Fig. 4c) suggest that the oxygen isotopic composition was partially buffered by pre-existing carbonate. This also suggests that the most $^{18}O$-depleted dolostones were at a high fluid/rock ratio. The assumption is consistent with the higher permeability of the quartz-rich dolostones and their hosting quartzite allowing enhanced infiltration of fluids having an external source of oxygen (i.e. not determined by interaction with carbonate).

A symmetrical depletion of the main dolostone body in $^{18}O$ towards the most permeable brecciated and sheared zones, as well as the depletion in $^{18}O$ towards both the upper and the lower contacts of the entire succession (Fig. 3b), is most likely the result of isotopic exchange between the carbonates and fluids with an external source of oxygen. The formation of chlorite veinlets in the sheared dolostones is additional evidence of such foreign fluids which might have been derived from a mafic source, i.e. underlying and overlying basalts. Interestingly, a sharp positive $\delta^{18}O$ offset documented in the middle part of the main dolostone body coincides with a similar offset of $\delta^{13}C$ (Fig. 2, offset 2). These offsets are considered to be of primary significance because neither of them is associated with any alteration features.

## 5. Significance of high $\delta^{13}C$ values

The KSF dolostones, like their chronostratigraphic analogues developed elsewhere (reviewed in Melezhik *et al.* 1999), have extreme $^{13}C$ enrichment. The formation of such $^{13}C$-rich dolostones has been ascribed to the global 2330–2060 Ma positive excursion of carbonate $^{13}C/^{12}C$ associated with enhanced accumulation of $C_{org}$ (Baker & Fallick 1989a, b; Karhu 1993). However, $\delta^{13}C$ of +5‰ to +9‰ documented throughout the succession cannot be balanced by organic carbon burial because the KSF dolostones and associated siliciclastic rocks contain no detectable amount of $C_{org}$. Like many other cases (reviewed in Melezhik *et al.* 1999), an external basin(s) would have to be invoked to provide an enhanced $C_{org}$ burial. However, it remains unclear whether the isotopic composition of the KSF dolostones represents a global background value for the 2330–2060 Ma Ga $^{13}C$-rich ocean or whether it was significantly modified by local factors associated with the closed/semiclosed lake environment. Theoretically, all combinations are possible because, for the oceanic and continental reservoirs, there is an interactive link through atmospheric $CO_2$.

In general, purely cyanobacterial mats are often characterised by very high organic productivity (Castenholz *et al.* 1992; Jørgensen *et al.* 1992). Consequently, the rate of biological uptake of $^{12}C$ is higher than the rate of carbon diffusion to the mat (Des Marais *et al.* 1992). As a result, the dissolved inorganic carbon reservoir can be extremely enriched in $^{13}C$ (Schidlowski *et al.* 1984). It is well known (e.g. Des Marais *et al.* 1992) that both $\delta^{13}C_{carb}$ and $\delta^{13}C_{org}$ of recent stromatolitic mats are typically enriched in $^{13}C$. This is also valid for recent calcified cyanobacteria. Many carbonates, which were precipitated on calcifying microbial mats in Australian lakes, have $\delta^{13}C$ of +5 to +10‰ (e.g. Burne & Moore 1987). Thus, a high rate of biological uptake of $^{12}C$ in shallow-water conditions, combined with lower energy settings, may lead to enrichment in $^{13}C$ of the whole water column.

The KSF contains abundant stromatolites formed by cyanobacteria. However, net bioproduction approximates to zero, and many carbonate lithologies are highly oxidised rocks (Melezhik & Fallick 2005). This makes the KSF fundamentally different to restricted basins with a high level of biological fixation of $C_{org}$ where $^{13}C$-rich carbonates (or their host) commonly contain sizeable amount of organic material (e.g. Bein 1986; Botz *et al.* 1988; Suchecki *et al.* 1988; Hollander & McKenzie 1991). Therefore, organic material produced by microbial communities in the Kuetsjarvi lake must have been continuously and efficiently removed. An assumption that all initial $C_{org}$ mass buried in the lake sediments might have been eventually removed in the course of sedimentation and/or post-depositional alteration raises three crucial questions: when, why and how did it happen?

In general, cyanobacterial and associated bacterial mats have a remarkable ability for rapid decomposition and recycling of the microbial biomass with almost zero net production (Jørgensen *et al.* 1992). Anaerobic (e.g. sulphate reduction) and aerobic respiration as well as methanogenesis are common processes leading to degradation of the microbial biomass produced. Recycling and subsequent loss of $C_{org}$ can be accomplished under a variety of conditions.

The first such scenario is when decomposed and recycled microbial biomass (e.g. degassed and dissolved) was converted

https://doi.org/10.1017/S0263593300001152 Published online by Cambridge University Press

to $CO_2$, $CH_4$ or to any other end-products, with the development of various fenestrae. Subsequently, these $^{12}C$-rich end-products might have been entirely or partially incorporated into newly formed carbonates or into earlier carbonate phases during the earliest stages of burial. Sulphate-rich lakes favour bacterial sulphate reduction, thus resulting in precipitation of isotopically light carbonates (Talbot & Kelts 1990). In sulphate-poor lakes, bacterial methanogenesis is the dominant process that results in formation of carbonates markedly enriched in $^{13}C$ (Talbot & Kelts 1990). This has been reported from several modern (e.g. Oberhänsli & Allen 1987; Botz *et al.* 1988; Talbot & Kelts 1990) and ancient lakes (Bellanca *et al.* 1989; Janaway & Parnell 1989). Surprisingly, comparative measurements of different carbonate phases from the KSF dolostones have shown that neoformed carbonates were neither depleted nor enriched in $^{13}C$ with respect to the primary phase (Melezhik & Fallick 2003). Thus, the first scenario does not appear to be valid for the KSF.

The second scenario envisages a situation when all end-products of the recycled organic material were removed from sediments and were efficiently mixed into the dissolved inorganic carbon pool, which, however, was not re-equilibrated with atmospheric $CO_2$. This would drive the dissolved inorganic carbon pool towards low $\delta^{13}C$ and result in the precipitation of $^{13}C$-depleted carbonates. A degree of depletion in $^{13}C$ will positively correlate with the level of bioproductivity and with the degree of decomposed organic material (e.g. McKenzie 1985). In fact, this is the most common scenario documented in many carbonate-precipitating lakes (McKenzie 1985; Bein 1986; Bellanca *et al.* 1989; Talbot 1990). However, the very high and relatively constant $\delta^{13}C$ values of the KSF dolostones suggest that this mechanism is not applicable to the Kuetsjärvi lake.

The third scenario envisages the situation when all end-products of the recycled organic material were removed from sediments and were efficiently mixed into the dissolved inorganic carbon pool, which, in turn, was subsequently and rapidly re-equilibrated with atmospheric $CO_2$. This would not cause any apparent differences in $\delta^{13}C$ obtained from the local and global reservoirs. However, such rapid exchange and isotopic re-equilibration has, to the present authors' knowledge, not been documented in either modern shallow-water, stromatolitic, hydrologically closed or partially closed environments (Burne & Moore 1987; Des Marais *et al.* 1992), or in modern and ancient shallow-water, non-stromatolitic, hydrologically closed and open, carbonate-precipitating lakes (e.g. McKenzie 1985; Oberhänsli & Allen 1987, Talbot 1990). Evidence of isotopic equilibrium between atmospheric $CO_2$ and dissolved inorganic carbon has been reported from a very few cases of Magadi-Natron stromatolites having $\delta^{13}C$ of +2·5‰; however, this could have been purely coincidental because the stromatolites contain $C_{org}$ and the vast majority of samples show $\delta^{13}C$ ranging from +3 to +5‰, thus they have not been precipitated in isotopic equilibrium with atmospheric $CO_2$ (Hillaire Marcel & Casanova 1987).

The fourth scenario, when end-products of the recycled organic material were efficiently and constantly removed from sediments and totally lost from the depositional system, may lead to a significant enrichment of the local carbon reservoir in $^{13}C$ with respect to the global reservoir. In this case, a global $\delta^{13}C$ value will be enhanced, and the isotopic composition of the KSF dolostones may not represent the global signal. Furthermore, isotopically light carbon that returned to the atmosphere might have caused a depletion of the atmosphere system in $^{13}C$ on a global scale; this is plausible because there are numerous such $^{13}C$-rich, $C_{org}$-poor carbonates in the Palaeoproterozoic (Melezhik *et al.* 1999). However, this would make an even greater difference between the local Kuetsjärvi and global isotopic signals.

Finally, a fifth possible scenario has been reported from Lake Bogoria in the Eastern African Rift, where stromatolites are extensively developed. They ring the whole $16 \times 2$ km basin and mark a mid-Holocene highstand of Lake Bogoria. Thickness varies from <1 to 50 cm. $\delta^{13}C_{carb}$ typically ranges from +5·5 to +7·5‰ (Aksnes & Talbot 1998). Lake Bogoria is a closed, saline, alkaline lake where $C_{org}$-poor, high $\delta^{13}C$ stromatolites formed because of a long residence time in a closed lake, and very low $CO_2$ activity in the high-pH waters. Under these conditions, photosynthesisers suffer extreme C-limitation, conditions favouring bacteria which can metabolise bicarbonate. The residual bicarbonate, after precipitation of aragonite and high magnesium calcite stromatolitic laminae, has very high $\delta^{13}C$ (M. R. Talbot, personal communication, 2002). Although the fate of $C_{org}$ initially produced by bacteria remains to be understood, it is very likely that dead organic material below the surface of active growth has been rapidly oxidised.

Tentatively, two final models can be applicable for the KSF carbonates, although discrimination between them is not possible on a quantitative basis. However, theoretical considerations, and the natural examples described above, suggest that, in both cases, the KSF dolostones may not represent a global signal because of an apparent $\delta^{13}C$ enhancement by locally developed high bioproductivity, enhanced uptake of $^{12}C$, and penecontemporaneous oxidation of organic material in cyanobacterial mats with the production and consequent loss of $CO_2$.

A further problem to be addressed is the significance of evaporitic features observed in several units in the KSF succession. Evaporitic conditions and a negative water balance seem to have appeared regularly through the lake history (Melezhik & Fallick 2005) and may have led to further modification of the carbon isotopic composition of ambient lake water. It has been reported that even in highly evaporated systems such as the coastal sabkhas of Abu Dhabi, Lake Lisan and the Dead Sea, carbonates have $\delta^{13}C$ generally ranging from negative to slightly positive (Parry *et al.* 1970; Bonatti *et al.* 1971; Katz *et al.* 1977). Layers of isotopically heavy aragonite or dolomite, and isotopically light calcite commonly occur in alternating beds in evaporitic settings. Friedman (1998) suggested that the $^{13}C$-rich carbonates formed via chemical precipitation during strong evaporation, whereas the calcite formed by bacterial decomposition of gypsum in which the lighter isotopes were derived from an organic carbon source (Feeley & Kulp 1957; Neev 1963).

A review of ancient evaporitic carbonates formed at times of known high sea water–$\delta^{13}C$ values (Melezhik *et al.* 1999) showed that Late Permian carbonates exhibit very high $\delta^{13}C$ values and clear evaporitic features. Several Late Permian palaeobasins marked by pronounced enrichment in $^{13}C$, including the Delaware, Zechstein and Sverdrup, are remarkably similar in that they were isolated, intra- or pericratonic depressions, intermittently connected with the open ocean, and marked by several episodes of evaporation, desiccation and progradation of carbonate platforms (Beauchamp *et al.* 1987). These authors have also suggested that the primary $^{13}C$ enrichment of the Late Permian carbonates (up to +7‰) in such basins, as compared to those precipitated in the coeval ocean (+1 to +3‰), may only be explained if a number of local factors were involved. Intense evaporation and $^{13}C$ enrichment of surficial brines through escape of $CO_2$ to the atmosphere during episodic closure of the basins was considered one of the factors which caused the formation of $^{13}C$-rich Late Permian carbonates.

**Table 3** Characteristic features of the Kuetsjärvi Sedimentary Formation dolostones versus various carbonate-precipitating lacustrine and marine depositional settings: (+) may occur within the depositional setting; and (−) atypical for the depositional setting

| Basinal environments | Sizeable thickness of carbonate rocks | Dolomite | Red beds | Hot-spring travertine | Low organic material | Flat-laminated stromatolites | Evaporites | High $\delta^{13}C_{carb}$ | Limited $\delta^{13}C_{carb}$ fluctuations |
|---|---|---|---|---|---|---|---|---|---|
| Hydrologically open lakes[1] | + | − | − | + | − | − | − | +* | − |
| Hydrologically closed lakes[2] | + | + | − | + | − | + | + | +* | + |
| Deep stratified lakes[3] | + | − | − | + | − | − | − | +* | − |
| Evaporative, alkaline, saline lakes[4] | − | + | + | + | − | + | + | +* | − |
| Continental playa-lakes[5] | + | + | + | + | + | + | + | +* | − |
| Coastal sabkha[6] | | + | − | + | − | + | + | +* | + |
| Pluvial lakes[7] | | + | | + | − | | + | +* | |
| Lagoon | + | + | − | − | − | + | + | +* | + |
| Open marine | + | − | − | − | − | − | − | +* | + |

*For periods with a global scale, high rate of $C_{org}$ burial.
[1] Stuiver (1970), Stiller & Magaritz (1974), Stiller & Hutchinson (1980), Turner & Fritz (1983), McKenzie (1985), Stiller & Kaufman (1985), Bein (1986), Abell & McClory (1986), Talbot (1990), Ricketts & Johnson (1996), Cohen *et al.* (1997), and Filippi *et al.* (1999).
[2]Rothe *et al.* (1974), Rothe & Hoefs (1977), Burne & Moore (1987), Bellanca *et al.* (1989), Nesbitt (1990), Talbot (1990), Talbot & Kelts (1990), Utrilla *et al.* (1998), and Fontes *et al.* (1996).
[3]Kelts & Hsü, K. J. (1978), Tietze *et al.* (1980), Botz *et al.* (1988), Suchecki *et al.* (1988), Janaway & Parnell (1989), and Talbot & Kelts (1990).
[4]Friedman (1965), Parry *et al.* (1970), Turovskiy & Sheko (1973), Katz *et al.* (1977), Schoell (1978), Eugster (1980), Botz & Von der Borch (1984), Renaut *et al.* (1986), Hillaire Marcel & Casanova (1987), Oberhänsli & Allen (1987), Rosen *et al.* (1988), Bell (1989), Braithwaite & Zedef (1996), Stein *et al.* (1997), Vasconcelos & McKenzie (1997), Aksnes & Talbot (1998), Friedman (1998), Finkelstein *et al.* (1999), and Trichet *et al.* 2001.
[5]Amiel & Friedman (1971), Eugster & Hardie (1975), Spencer *et al.* (1984), McKenzie & Eberli (1987), Suchecki *et al.* (1988), and Janaway & Parnell (1989).
[6] Levy (1977), Handford (1981), McKenzie (1981), Patterson & Kinsman (1982), and Müller *et al.* (1990).
[7] Reeves & Parry (1965), and DeHon (1967).

From sedimentological and palaeoenvironmental points of view (Melezhik & Fallick 2005), the KSF succession resembles those deposited in Late Permian time. Thus, intense evaporation, similar to the Permian closed basins, is considered to be one of the possible factors which might have further enhanced the global $\delta^{13}C$ signal in the Kuetsjärvi lake dolostones. However, the available data do not allow a quantitative evaluation of this process.

Table 3 summarises varieties of lacustrine and non-lacustrine depositional settings in which deposition of carbonates may take place. Although terms used for classification of the lacustrine basins are not mutually exclusive, Table 3 serves the present authors' purpose by illustrating which depositional settings match major characteristics of the KSF dolostones. Table 3 suggests that neither recent non-marine nor marine depositional settings, if considered alone, satisfy the most prominent features of the KSF dolostones. The most crucial among them is a combination of high and rather uniform $\delta^{13}C$ values, extremely low S and $C_{org}$ content, and abundant travertine deposits and 'red beds'. Thus, based on the isotopic constraints, an evaporative, alkaline lake, or continental playa-lake, or coastal sabkha can serve as modern analogues for the Palaeoproterozoic Kuetsjärvi basin. These depositional settings allow formation of non-marine carbonates coupled with the efficient removal of $C_{org}$ by subaerial oxidation. Similar conclusions on the depositional setting have been reached based on purely sedimentological data (Fig. 13 in Melezhik & Fallick 2005). The removal of $C_{org}$ by oxidation implies a rather elevated $pO_2$ of the atmosphere, which is witnessed by the world-wide development of terrestrial 'red beds' occurring prior to and synchronously with the Jatulian–Lomagundi isotopic event at around 2330–2060 Ma ago (e.g. Melezhik *et al.* 1999). Bekker *et al.* (2004) have recently corroborated a significant rise of atmospheric oxygen occurring by 2320 Ga.

However, it remains to be understood why the $\delta^{13}C$ of these lacustrine dolostones shows very little variation through time, which is a feature of an open marine environment.

## 6. Interpretation of $\delta^{13}C$ and $\delta^{18}O$ variations

In lake environments, $\delta^{13}C$ and $\delta^{18}O$ variation and covariant $\delta^{13}C$–$\delta^{18}O$ trends are interpreted as a result of inflow-evaporation balance. Temperature effects, which control the isotopic composition of meteoric water (Dansgaard 1964) and isotopic fractionation during carbonate precipitation (O'Neil *et al.* 1969), are apparently of secondary significance in hydrologically closed basins (Talbot 1990). Temperature effects tend to be generally subordinate to evaporative- and residence-related effects (e.g. Stuiver 1970). A high level of covariance between $\delta^{13}C$ and $\delta^{18}O$ has been considered to be most typical of carbonates precipitated in hydrologically closed lakes (reviewed by Talbot 1990).

Despite the partial decoupling between the carbon and oxygen isotopic systems during the post-depositional history of the KSF, the level of positive correlation between $\delta^{13}C$ and $\delta^{18}O$ remains significant, ranging in different parts of the succession from 0·52 to 0·77 (Fig. 4d). The correlation seems to reflect a depositional trend because $\delta^{13}C$ values were not significantly overprinted during the post-depositional alteration. Thus, the positive correlation is considered to be indicative of a closed or partially closed lacustrine environment, which is also in agreement with the sedimentological data (Melezhik & Fallick 2005).

Since hot-water spring travertine deposits are abundant in the KSF (Melezhik & Fallick 2001), hydrothermal activity should have played an important role in the inflow–evaporation balance of the Kuetsjärvi lake water, similar to many rift-bound lakes (e.g. Hillaire-Marcel & Casanova 1987; Renaut & Tiercelin 1993). Furthermore, the Kuetsjärvi hot-water springs transported $CO_2$ of likely volcanogenic origin with an initial $\delta^{13}C$ value of ca. −6‰ (Melezhik & Fallick 2001). Thus, an additional, important feature of the hydrothermal waters feeding the Kuetsjärvi lake was their high potential to influence and modify the isotopic composition of the $^{13}C$-rich ambient lake water. Such influence can be invoked to

https://doi.org/10.1017/S0263593300001152 Published online by Cambridge University Press

explain middle-scale trends and small-scale fluctuations of $\delta^{13}C$ documented in the KSF.

Similarly to modern, hydrothermally influenced, rift-bound lakes (e.g. Renaut *et al.* 1986; Renaut & Owen 1988), hydrothermal systems of variable temperature and water chemistry could have been functioning episodically and asynchronously across the Kuetsjärvi lake, resulting in rather complex temporal and spatial isotopic patterns of precipitated carbonates.

### 6.1. Stratigraphic variations of $\delta^{13}C$

Excursion 2 starts within a travertine-free section and is marked by the highest $\delta^{13}C > +8‰$ (Fig. 2), which was apparently driven by global factors enhanced by evaporation. A gradual upward-depletion in $^{13}C$ of precipitated carbonates coincides with the appearance of travertine deposits (Fig. 2), and thus, it is tentatively interpreted to have been caused by a gradually increased mixing between $^{13}C$-rich ambient lake waters and $^{12}C$-rich hydrothermal waters.

The positive $\delta^{13}C$ shift at the base of Excursion 3 is associated with decreased volume of travertines (Fig. 2), and, thus, suggests a relatively reduced input from the $^{12}C$-rich source. However, Excursion 3 starts with a lower $\delta^{13}C$ value, as compared with Excursion 2, suggesting that, at that time, the ambient lake water accumulated a higher proportion of $^{12}C$-rich hydrothermal waters. Four short-term, prominent departures towards low $\delta^{13}C$ values within Excursion 3 perfectly correspond with travertine beds (Fig. 2), again indicating the increased influence from the $^{12}C$-rich source. One $^{13}C$- and $^{18}O$-rich outlier is considered to represent an exceptionally high evaporitic environment.

The sharp positive $\delta^{13}C$ shift at the base of Excursion 4 is apparently associated with abruptly increased evaporation and biological uptake of $^{12}C$, as indicated by widely spread red, desiccated, flat-laminated microbialites with dolomite-pseudomorphed micronodules of apparent sulphates (Fig. 2) in a playa lake environment (Melezhik & Fallick 2005).

The starting $\delta^{13}C$ value of Excursion 4 is lower as compared to the starting point of Excursion 3. Excursion 4 is markedly distinguished from all previous excursions by a rather rapid and considerable lowering of carbonate $\delta^{13}C$ with time. This does not correspond with a volume of travertine deposits recorded in the upper part of Unit X (Fig. 2). On the other hand, similarly to modern rift-bound lakes (e.g. Renaut & Tiercelin 1993), springs could have been operating at that time at different locations, providing the necessary $^{12}C$-rich source for the entire lake system. However, mixing with $^{12}C$-rich hydrothermal waters cannot explain the corresponding increase of the Sr concentration (Fig. 3a) since Sr contents are low in the travertine dolomite (Table 2). Hence, the increased inflow of $^{12}C$-rich hydrothermal waters cannot be considered as the cause of this negative shift of $\delta^{13}C$. Tentatively, a short-term invasion of sea water to the rift-bound, closed, Kuetsjarvi basin is suggested to be the cause of rapid lowering of carbonate $\delta^{13}C$ in the uppermost part of the KSF. Consequently, $\delta^{13}C$ around +5‰ might be considered as the proxy to the coeval open marine signal.

### 6.2. Lateral variations of $\delta^{13}C$

Sixty-nine analyses from surface outcrops incorporated from previous studies (Melezhik & Fallick 1996), together with the data from DHX show that $\delta^{13}C$ ranges from −2 to +9·6‰ over a distance of 150 km of the strike length (Fig. 6). Three sampling sites (4, 5 and 6) are located in the biotite–actinolite metamorphic facies, three others (2, 3 and 8) are in the transition to the epidote–amphibolite facies, whereas four sampling sites (1, 7, 9 and 10) are situated in the epidote–amphibolite facies (Fig. 6). Note that only sample site 6 (DH6) represents the entire thickness of the KSF.

The transition from biotite–actinolite to epidote–amphibolite facies is defined by dolomite +quartz→ tremolite+calcite$_2$ ± dolomite ± calcite$_1$ (Melezhik *et al.* 2003). The authors reported that the transition is characterised by the formation of calcite$_2$ and recrystallisation of calcite$_1$ and dolomite, and defined by $^{13}C$ depletion of calcite$_2$ (≈3·0‰) and calcite$_1$ (1·0–2·0‰) associated with a Rayleigh distillation process. The dolomite is depleted in $^{13}C$ by less than 1‰. The depletion in $^{13}C$ below these limits was caused by isotopic exchange between the carbonates and fluid with an external source of carbon, or mixing with internal non-carbonate fluids (Melezhik *et al.* 2003). Thus, the metamorphic processes and associated fluids were responsible for $^{13}C$ depletion of the carbonates in sites 1 and 7–10 (Fig. 6).

However, the dolostones from sites 2 and 3, representing the transition to the epidote–amphibolite facies, contain samples with $\delta^{13}C$ close to +10‰. These values are higher than those obtained from the lower metamorphic grade sites 4–6 (Fig. 6). Consequently, metamorphic processes cannot account for such $\delta^{13}C$ dichotomy, and syndepositional processes, such as evaporative or biologically driven enhancement, should be invoked for $^{13}C$ enrichment. Although the high $^{13}C$ data in sites 2 and 3 are limited to two samples, taking into consideration a biased sampling on the surface and the fact that the two $^{13}C$-rich sites do not represent the entire formational thickness, more $^{13}C$-rich samples can be expected. This inference is also supported by histograms of $\delta^{13}C$ from sites 2 and 3 which are each skewed towards higher values (Fig. 6).

## 7. Significance of $^{87}Sr/^{86}Sr$ ratios

The $^{87}Sr/^{86}Sr$ ratios show a wide variation (0·70406–0·70623), with high $^{87}Sr/^{86}Sr$ values located in the lower and middle parts of the sequence (Table 2). The high $^{87}Sr/^{86}Sr$ fluctuation may suggest post-depositional resetting. This is also consistent with the strong negative correlation ($r = -0·89$, >99·9%) between $^{87}Sr/^{86}Sr$ ratios and Sr concentrations. However, the alteration scenario is in conflict with the significant positive correlation between $^{87}Sr/^{86}Sr$ ratios and $\delta^{13}C$ ($r = 0·83$, >99·0%) and $\delta^{18}O$ ($r = 0·86$, 99·9%). It is also in conflict with the negative correlation between $^{87}Sr/^{86}Sr$ ratios and the Mn concentration ($r = 0·76$, >99·0%), which is the opposite of what should be expected in altered samples (e.g. Veizer 1989). Thus, the present authors suggest that, given the difference in the stratigraphic position of the high and low $^{87}Sr/^{86}Sr$ ratios, there are apparently two different subsets of carbonates which were originally precipitated from significantly different fluids.

The strontium isotopic composition of the lower and middle dolostone units of the KSF (0·70585–0·70623) is comparable with that obtained from the assumed correlative Tulomozerskaya Formation (Akhmedov *et al.* 2002) in which initial $^{87}Sr/^{86}Sr$ ratios of restricted marine and non-marine dolomites (Melezhik *et al.* 2000) range between 0·70512 and 0·70668 (Gorokhov *et al.* 1998). In terms of trace elements, the KSF samples do not show a higher rank of post-depositional alteration than the Tulomozerskay Formation dolostones (Mn/Sr = 0·05–2·3, Sr = 64–115; Gorokhov *et al.* 1998). Consequently, the 0·70560–0·70623 of the lower and middle dolostones of the KSF may reflect the Sr composition of the parental non-marine solution. Therefore, the present authors tentatively suggest that essentially continental water was the parental solutions because it is commonly characterised by high $^{87}Sr/^{86}Sr$ ratios (cf. Wadleigh *et al.* 1985; Goldstein & Jacobsen 1987; Veizer 1989; Palmer & Edmond 1989). These

https://doi.org/10.1017/S0263593300001152 Published online by Cambridge University Press

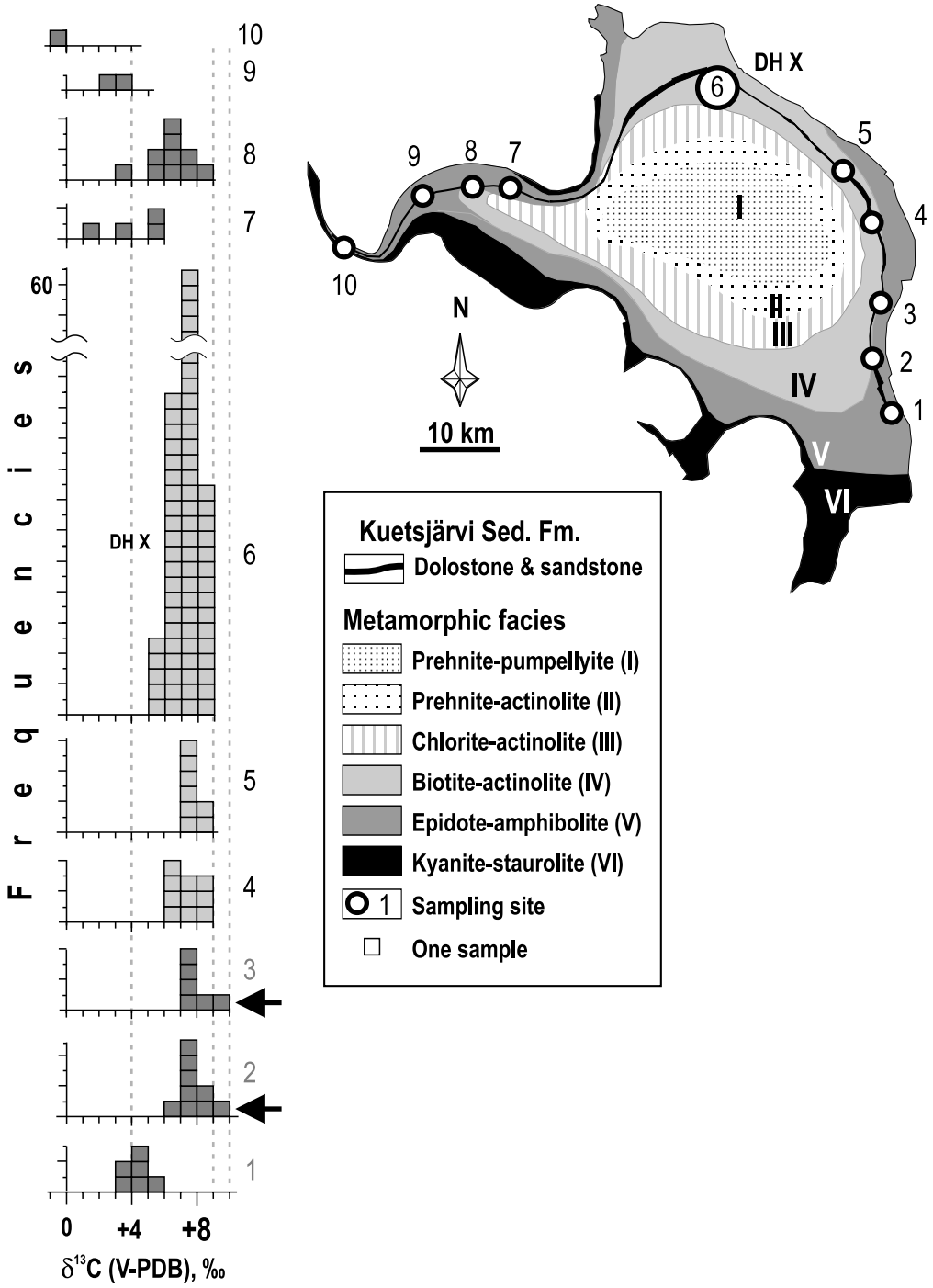


**Figure 6** Metamorphic zoning of the Pasvik-Pechenga Greenstone Belt (modified from Petrov & Voloshina 1995), location of the sampling sites and histograms of $\delta^{13}C_{carb}$ values obtained from the Kuetsjärvi Sedimentary Formation carbonates by previous (Melezhik & Fallick 1996; Melezhik *et al*. 2003) and present studies. The black arrows indicate $\delta^{13}C > +9‰$ in dolostones from the epidote–amphibolite facies.

$^{87}Sr$-rich waters may have been influenced by the 2000-m-thick continentally derived (Melezhik & Sturt 1994) basaltic andesites (Sr>400 ppm; Balashov 1995), which have a low initial $^{87}Sr/^{86}Sr$ ratio of 0·70415 (Balashov 1995). It is assumed that mixing between the high-$^{87}Sr$ and low-$^{87}Sr$ sources might have resulted in a moderate $^{87}Sr/^{86}Sr$ ratio of the ambient lake water, and consequently, the dolostones of the lower and middle part of KSF.

The strontium isotopic composition of the upper dolostones of the KSF (0·70406–0·70486) is comparable with that obtained from the marine dolostones of the assumed correlative Tulomozerskaya Formation (0·70343–0·70419; Gorokhov *et al*. 1998). The least radiogenic value of 0·70406 obtained for the KSF cannot be explained by additional enhancement from the volcanic rocks because they have even lower initial values (0·70415). It also cannot be explained by the enhanced influence of hydrothermal waters because they precipitated low-Sr travertines (Sr = 10–100 ppm) which have $^{87}Sr/^{86}Sr$ ratios ranging from 0·7057 to 0·7068. Finally, the significant drop in the $^{87}Sr/^{86}Sr$ ratio of the uppermost dolostones might indicate a short-term invasion of marine water to the Kuetsjärvi rift-bound lake just prior to the voluminous eruption of the overlying volcanic rocks. Considering that sea water has an order of magnitude higher Sr concentration than meteoric waters, even a small portion of sea water may result in a $^{87}Sr/^{86}Sr$ signal close to marine (e.g. Veizer & Compston 1974).

https://doi.org/10.1017/S0263593300001152 Published online by Cambridge University Press

The scenario of short-term invasion of marine water to the Kuetsjärvi rift-bound lake is also consistent with the negative shift of $\delta^{13}C$, as discussed in the previous sections.

## 8. Regional implications

The KSF is the second stratigraphic unit after the Tulomozerskaya Formation (Melezhik *et al*. 1999, 2000) on the Fennoscandian Shield that has been subject to detailed C, O and Sr isotopic studies. Although precise radiometric age constraints are not available for either of these formations, they have been considered to be correlative, and represent the Jatulian parastratotype and stratotype sections for the Kola and Karelian regions. In present-day terms, these two formations are separated by a distance of over 600 km (Fig. 1), and by complex geology and structure, and are considered to have been formed in separate basins (Melezhik *et al*. 1997). These c. 2200 Ga basins were located on either side of an apparent, SE–NW-trending, >600-m-wide, shallow epicontinental sea (Ojakangas *et al*. 2001) that originally formed on the continental crust that experienced a c. 2000 Ga oceanic separation (Daly *et al*. 2001, Fig. 1). There are no robust data suggesting that these two basins were entirely synchronous. However, if they were, then the thin sedimentary unit deposited in the Kuetsjärvi lake requires a much lower subsidence rate compared to that of the Tulomozero basin. An additional difference arises from the active volcanic setting of the Kuetsjärvi rift-bound lake, whereas its Karelian counterpart received negligible volcanic influence.

The Tulomozerskaya Formation comprises a 800-m-thick magnesite-stromatolite-dolostone-'red bed' sequence accumulated in a rift-bound lagoon on the south-eastern margin of the Archaean craton (Melezhik *et al*. 2000). The lowermost quartzitic sandstones (members A and B; Fig. 7) represent a braided fluvial system over a lower-energy, river-dominated coastal plain. 'Red beds', forming the middle part of the sequence (members A and C), were deposited in a low-energy, intertidal setting such as a protected barred lagoon or bight. Member E 'red beds' were accumulated in a playa lake environment. A significant part of members A–D and F–H comprises flat-laminated stromatolitic dolostones accreted in either ephemeral ponds in peritidal zones, or coastal sabkhas and playa lakes. The red colouration of the stromatolites indicates their frequent exposure to air. The presence of tepees, mudcracks, pseudomorphs after calcium sulphate, halite casts and abundant 'red beds' is indicative of the dominance of terrestrial rather than aqueous environments. Several beds comprise biothermal and biostromal stromatolites which have been accreted in settings ranging from shallow-water, low-energy, intertidal through barred evaporitic lagoonal to peritidal evaporitic environments. Only a small proportion of dolostones, developed in the middle part of Member B, at the base of Member D, and particularly, in Member G (Fig. 7), were deposited in relatively open marine environments (Melezhik *et al*. 2000).

The detailed isotopic data available from the previous (Gorokhov *et al*. 1998; Melezhik *et al*. 1999, 2000) and present studies permit a direct isotopic comparison between the two supposedly correlative successions. The isotopic signatures of these two formations are not compatible (Fig. 7), with the possible exception of their uppermost parts. Obviously, the formations are of dramatically different thicknesses, but the C-isotope data rule out the possibility that the KSF is a highly condensed equivalent of the Tulomozerskaya Formation. Importantly, the carbon and strontium isotopic record of the uppermost part of the KSF overlaps with those of the members G–H transition of the Tulomozerskaya succession (Fig. 7), suggesting that the carbonates were deposited from similar fluids. Notably, members B and G–H are the only rocks in the Tulomozerskaya succession to have been assigned an open, shallow-water, marine environment (Melezhik *et al*. 2000).

Thus, the isotopic data suggest three possibilities. First, the two formations are not coeval if their carbonates formed from sea water. Secondly, the carbonates of these two formations formed more or less synchronously, but one or both do not reflect the isotopic composition of coeval sea water. Finally, only the uppermost parts of these formations, representing similar $\delta^{13}C$ and $^{87}Sr/^{86}Sr$ trends, might have been precipitated in isotopic equilibrium with coeval sea water. If two formations are plotted to inferred time-scale, the $\delta^{13}C$ and $^{87}Sr/^{86}Sr$ trends of the KSF show similarities to Member F–H of the Tulomozerskaya Formation (Fig. 7, insets). In both cases, the dolostones are characterised by the lowest $\delta^{13}C$ (+5 to +6‰) and $^{87}Sr/^{86}Sr$ (0·70343–0·70406) ratios. Consequently, the isotopic composition of the coeval c. 2·2 Ga Palaeoproterozoic sea water is considered to be either equal to or below these values.

## 9. Conclusions

The c. 2·3 Ga, 150-m-thick KSF, consisting of coastal deltaic and shallow lacustrine mixed carbonate–siliciclastic sediments, represents one of the world's best developed and preserved sequences deposited during a time of significant perturbation of the global carbon cycle.

With the exception of some de-dolomitised rocks, all other lithological varieties, including microbiolites and travertine deposits, are composed of dolomite. The bulk chemistry is controlled by clastic quartz (0·5–53·5 wt.% $SiO_2$) and sericite (0·01–5·5 wt.% $Al_2O_3$). The siliciclastic rocks and dolostones are devoid of $C_{org}$. High Sr concentrations (51–1069 ppm) and low Mn/Sr ratios ($2·9 \pm 2·1$) of the dolostones do not suggest significant post-depositional alteration.

The entire carbonate succession, excluding the travertines, shows high $\delta^{13}C$ ($+7·5 \pm 0·6$‰) with a narrow range (+5·8 to +8·9‰) that was not controlled by post-depositional processes. Strongly fluctuating $\delta^{18}O$ (10·8–20·4‰) was overprinted during diagenesis within permeable sandstone beds, as well as during regional greenschist-grade and later retrograde metamorphism. The $^{87}Sr/^{86}Sr$ ratio ranges from 0·70406 to 0·70623.

The formation of $^{13}C$-rich, $C_{org}$-free dolostones in the Kuetsjärvi basin is ascribed to the global 2·4–2·06 Ga positive excursion of carbonate $^{13}C/^{12}C$; if there was associated enhanced accumulation of $C_{org}$ it occurred in an external basin. High positive $\delta^{13}C$-$\delta^{18}O$ correlation ($r=0·52–0·77$) is indicative of a closed lacustrine environment. Several short-term stratigraphic excursions of $\delta^{13}C$ have been apparently governed by evaporation, and biological uptake of $^{12}C$ combined with the influence of $^{12}C$-rich hydrothermal waters delivered to the lake by travertine-depositing springs. The lateral depletion in $^{13}C$ of carbonates across the Pechenga Belt was largely controlled by metamorphic reactions in the transition from biotite–actinolite to epidote–amphibolite facies.

The most significant lowering of $\delta^{13}C$ (down to +5·8‰) and $^{87}Sr/^{86}Sr$ (down to 0·70407) is assigned to a short-term invasion of sea water into the lake. Although the $^{13}C$-rich nature of the KSF dolostones reflects the global isotopic signal (apparently around +5‰), it was, however, enhanced by locally developed evaporation, high bioproductivity, enhanced uptake

https://doi.org/10.1017/S0263593300001152 Published online by Cambridge University Press

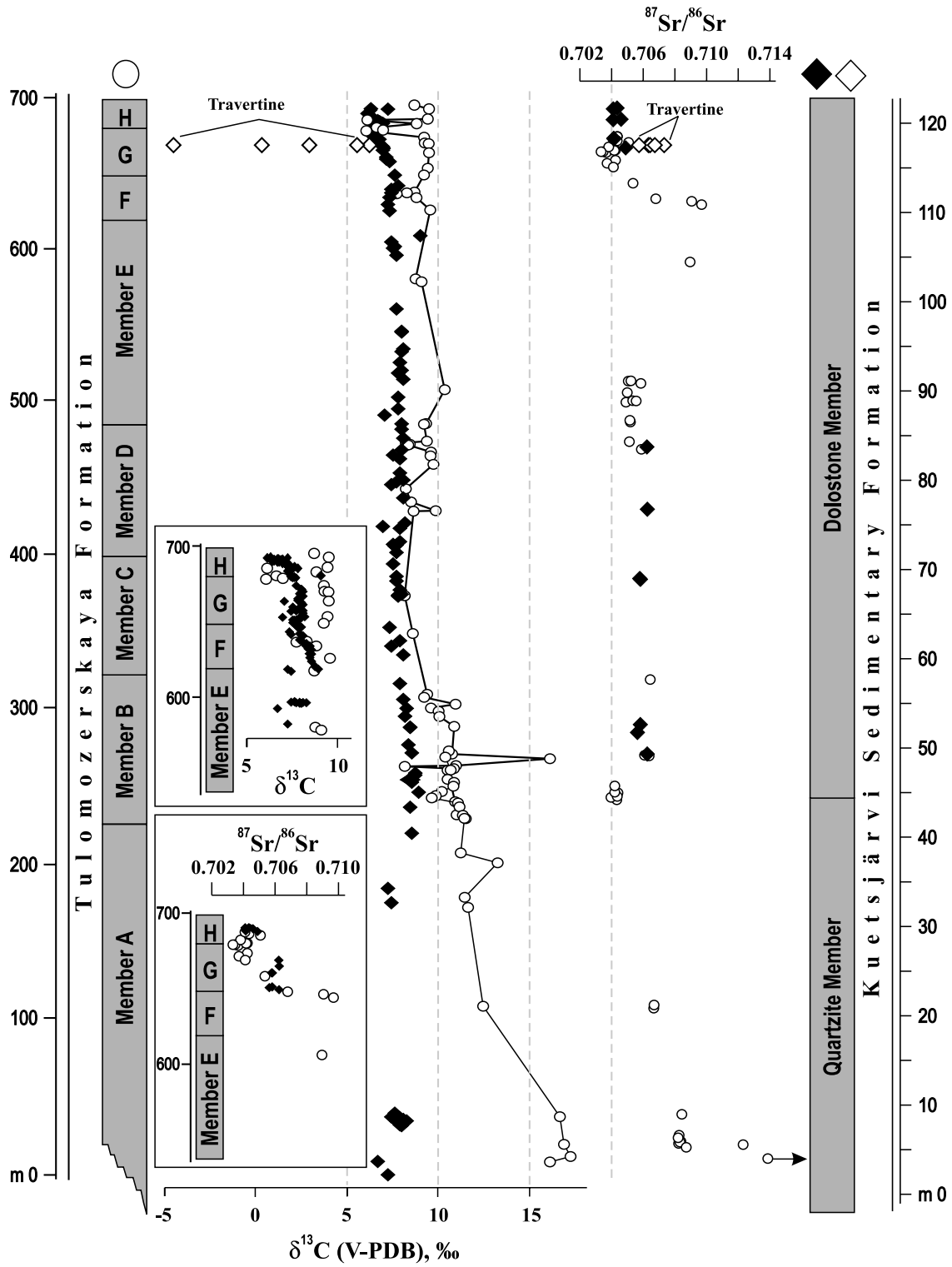


**Figure 7** Stratigraphic trends of $\delta^{13}C_{carb}$ and $^{87}Sr/^{86}Sr$ values between the purportedly correlative Tulomozerskaya and Kuetsjärvi Sedimentary formations. Insets show trends if the Tulomozerskaya and Kuetsjärvi Sedimentary formations are plotted to an inferred time-scale. Strontium isotope data for the Tulomozerskaya Formation are from Gorokhov *et al.* (1998). See text for discussion.

of $^{12}C$ and penecontemporaneous oxidation of organic material in cyanobacterial mats, with the production and consequent loss of $CO_2$ in subaerial and shallow-water lacustrine environments.

The carbon and strontium isotope stratigraphy suggests that the bulk carbonates of the KSF and its Jatulian correlative in Karelia apparently do not reflect the isotopic composition of coeval sea water. The upper portions of both formations suggest the best proxy to $\delta^{13}C$ and $^{87}Sr/^{86}Sr$ of coeval sea water to be around +5‰ and 0·70340–0·70400, respectively.

## 10. Acknowledgements

The present article reports the results obtained by the international research group working in the framework of a project entitled 'World-wide 2 billion-year-old positive carbon isotopic excursion: the evolutionary significance and driving forces'. This research has been supported by INTAS-RFBR 95–928. The fieldwork has been financed by the IGCP project 408 and the Geological Survey of Norway, project 282200. The Scottish Universities Environmental Research Centre (SUERC) has

https://doi.org/10.1017/S0263593300001152 Published online by Cambridge University Press

been supported by the Consortium of Scottish Universities and the Natural Environment Research Council. The laboratory work and isotope study was financed by the NGU (project 99.103), SUERC and the Russian Federation of Basic Research (project 00–05–64915). Access to core material of the Central Kola Prospecting Expedition is acknowledged with thanks. A. Lepland is thanked for comments on an earlier version of the manuscript. M. Talbot provided unpublished isotopic data on recent stromatolites from restricted basins in the East African Rifts. Official referees A. Prave and M. Talbot are thanked for their constructively critical reviews and for their efforts to make the manuscript intelligible.

## 11. References

Abell, P. I. & McClory, J. P. 1986. Sedimentary carbonates as isotopic marker horizons at Lake Turkana, Kenya. *In* Frostick, L. E., Renaut, R. W., Reid, I. & Tiercelin, J. J. (eds) *Sedimentation in the African rifts. Geological Society of London, Special Publication* **25**, 153–8.

Akhmedov, A. M., Bibikova, E. B., Bogdanov, Yu. B., Glebovitsky, B. A., Zhulanov, I. L., Mitrofanov, F. P., Negrutza, V. Z., Negrutza, T. F., Pavlov, V. A., Petrov, B. V., Petrov, B. M., Robonen, W. I., Semikhatov, M. A., Filatova, L. I., Tcherkasov, P. F. & Schuldiner, V. I. 2002. *A general stratigraphic scale of the early Precambrian of Russia. Explanatory note*. Apatity: Kola Science Centre. [In Russian.]

Akhmedov, A. M., Krupenik, V. A., Makarikhin, V. V. & Medvedev, P. V. 1993. *Carbon isotope composition of carbonates in the early Proterozoic sedimentary basins.* Printed report. Petrozavodsk: Institute of Geology of the Karelian Scientific Centre. [In Russian.]

Aksnes, J. L. & Talbot, M. R. 1998. Paleoenvironmental significance of Holocene microbialites from Lake Bogoria, Kenya. Abstract. *In* Canaveras, J. C., Garcia-del-Cura, M. A., Soria, J., Melendez-Hevia, A. & Soria, A. R. (eds) *15th International Sedimentological Congress; Sedimentology at the Dawn of the Third Millennium*, p. 123. Alicante: ISC.

Amiel, A. J. & Friedman, G. M. 1971. Continental sabkha in Arava valley between Dead Sea and Red Sea; significance for origin of evaporites. *American Association of Petroleum Geologists Bulletin* **55**, 581–92.

Baker, A. J. & Fallick, A. E. 1989a. Evidence from Lewisian limestone for isotopically heavy carbon in two-thousand-million-year-old sea water. *Nature* **337**, 352–4.

Baker, A. J. & Fallick, A. E. 1989b. Heavy carbon in two-billion-year-old marbles from Lofoten-Vesterålen, Norway: implications for the Precambrian carbon cycle. *Geochimica et Cosmochimica Acta* **53**, 1111–15.

Balashov, Yu. A. 1995. Geochronology of Palaeoproterozoic rocks of the Pechenga-Varzuga structure, Kola Peninsula. *Petrology* **4**, 3–25. [In Russian.]

Banner, J. L. & Hanson, G. N. 1990. Calculations of simultaneous isotopic and trace element variations during water-rock interaction with application to carbonate diagenesis. *Geochimica et Cosmochimica Acta* **54**, 3123–38.

Beauchamp, B., Oldershaw, A. E. & Krouse, R. 1987. Upper Carboniferous to Upper Permian $^{13}$C-enriched primary carbonates in the Sverdrup Basin, Canadian Arctic: comparisons to coeval western North American ocean margins. *Chemical Geology* **65**, 391–413.

Bein, A. 1986. Stable isotopes, iron and phosphorous in a sequence of lacustrine carbonates; paleolimnic implications. *Chemical Geology* **4**, 305–13.

Bekker, A., Kaufman, A. J., Karhu, J. A., Beukes, N. J., Swart, Q. D., Coetzee, L. L. & Eriksson, K. A. 2001. Chemostratigraphy of the Paleoproterozoic Duitschland Formation, South Africa; implications for coupled climate change and carbon cycling. *American Journal of Science* **301**, 261–85.

Bekker, A. Karhu, J. A., Eriksson, K. A. & Kaufman, A. J. 2003. Chemostratigraphy of Palaeoproterozoic carbonate successions of the Wyoming Craton: tectonic forcing of biogeochemical change? *Precambrian Research* **120**, 279–325.

Bekker, A., Holland, H. D., Wang, P.-L., Stein, H. J., Hannah, J. L., Coetzee, L. L. & Beukes, N. J. 2004. Dating the rise of atmospheric oxygen. *Nature* **427**, 117–20.

Bell, C. M. 1989. Saline lake carbonates within an Upper Jurassic-Lower Cretaceous continental red bed sequence in the Atacama region of northern Chile. *Sedimentology* **36**, 651–63.

Bellanca, A., Calvo, J. P., Censi, P., Elizaga, E. & Neri, R. 1989. Evolution of lacustrine diatomite carbonate cycles of Miocene age, southeastern Spain: petrology and isotope geochemistry. *Journal of Sedimentary Petrology* **59**, 45–52.

Bonatti, C., Emiliani, C., Ostlund, G. & Rydel, H. 1971. Final desiccation of the Afar Rift, Ethiopia. *Science* **172**, 468–9.

Botz, R., Stoffers, P., Faber, E. & Tietze, K. 1988. Isotope geochemistry of carbonate sediments from Lake Kivu (East-Central Africa). *Chemical Geology* **69**, 299–308.

Botz, R. W. & Von der Borch, C. C. 1984. Stable isotope study of carbonate sediments from the Coorong area, South Australia. *Sedimentology* **31**, 837–49.

Braithwaite, C. J. R. & Zedef, V. 1996. Hydromagnesite stromatolites and sediments in an alkaline lake, Salda Golu, Turkey. *Journal of Sedimentary Research* **66**, 991–1002.

Brand, U. & Veizer, J. 1980. Chemical diagenesis of multicomponent carbonate system – 1. Trace elements. *Journal of Sedimentary Petrology* **50**, 1219–50.

Buick, I. S., Uken, R. Gibson, R. L. & Wallmach, T. 1998. High-$\delta^{13}$C Paleoproterozoic carbonates from the Transvaal Supergroup, South Africa. *Geology* **26**, 875–8.

Burne, R. V & Moore, L. S. 1987. Microbiolites: organosedimentary deposits of benthic microbial communities. *Palaeogeography, Palaeoclimatology, Palaeoecology* **2**, 241–54.

Castenholz, R. W., Bauld, J. & Pierson, B. K. 1992. Photosynthetic activity in modern microbial mat-building communities. *In* Schopf, J. W. & Klein, C. (eds) *The Proterozoic biosphere*, 279–85. Cambridge: Cambridge University Press.

Cohen, A. S., Talbot, M. R., Awramik, S. M., Dettman, D. L. & Abell, P. 1997. Lake level and paleoenvironmental history of Lake Tanganyika, Africa, as inferred from late Holocene and modern stromatolites. *Geological Society of America Bulletin* **109**, 444–60.

Daly, J. S., Balagansky, V. V., Timmerman, M. J., Whitehouse, M. J., de Jong, K., Guise, P., Bogdanova, S., Gorbatschev, R. & Bridgwater, D. 2001. Ion microprobe U-Pb zircon geochronology and isotopic evidence for a trans-crustal suture in the Lapland-Kola Orogen, northern Fennoscandian Shield. *Precambrian Research* **105**, 289–314.

Dansgaard, W. 1964. Stable isotopes in precipitation. *Tellus* **XVI**, 438–68.

DeHon, R. A. 1967. Minor elements in pluvial lake carbonates of West Texas. *Compass of Sigma Gamma Epsilon* **44**, 148–51.

Derry, L. A., Kaufman, A. J. & Jacobsen, S. B. 1992. Sedimentary cycling and environmental changes in the Late Proterozoic: evidence from stable and radiogenic isotopes. *Geochimica et Cosmochimica Acta* **56**, 1317–29.

Des Marais, D. J., Bauld, J., Palmisano, A. C., Summons, R. E. & Ward, D. M. 1992. The biochemistry of carbon in modern microbial mats. *In* Schopf, J. W. & Klein, C. (eds) *The Proterozoic biosphere*, 299–308. Cambridge: Cambridge University Press.

Eugster, H. P. 1980. Lake Magadi, Kenya, and its precursors. *In* Nissenbaum, A. (ed.) *Hypersaline brines and evaporitic environments. Developments in Sedimentology* **28**, 195–232.

Eugster, H. P. & Hardie, L. A. 1975. Sedimentation in an ancient playa-lake complex; the Wilkins Peak Member of the Green River Formation of Wyoming. *Geological Society of America Bulletin* **86**, 319–34.

Feely, H. W. & Kulp, J. L. 1957. The origin of Gulf Coast Salt Dome sulphur deposits. *American Association of Petroleum Geologists Bulletin* **41**, 1802–53.

Filippi, M. L., Lamber, P., Hunziker, J., Kueble, B. & Bernasconi, S. 1999. Climatic and anthropogenic influence on the stable isotope record from bulk carbonates and ostracodes in Lake Neuchatel, Switzerland, during the last two millennia. *Journal of Paleolimnology* **21**, 19–34.

Finkelstein, D. B., Hay, R. L. & Altaner, S. P. 1999. Origin and diagenesis of lacustrine sediments, upper Oligocene Creede Formation, southwestern Colorado. *Geological Society of America Bulletin* **111**, 1175–91.

Fontes, J. C., Gasse, F. & Gibert, E. 1996. Holocene environmental changes in Lake Bangong Basin (western Tibet); Part 1, Chronology and stable isotopes of carbonates of a Holocene lacustrine core. *In* Gasse, F. & Derbyshire, E. (eds) *Environmental issues in the Tibetan Plateau and surrounding areas. Palaeogeography, Palaeoclimatology, Palaeoecology* **120**, 25–47.

Friedman, G. M. 1965. On the origin of aragonite in the Dead Sea. *Israel Journal of Earth-Sciences, Issue on Carbonate Petrology* **14**, 79–85.

Friedman, G. M. 1998. Temperature and salinity effects on $^{18}O$ fractionation of rapidly precipitated carbonates: laboratory experiments with alkaline lake water – perspective. *Episodes* **21**, 97–8.

Goldstein, S. J. & Jacobsen, S. B. 1987. The Nd and Sr isotopic systematics of river-water dissolved material; implications for the sources of Nd and Sr in seawater. *Chemical Geology* **66**, 245–72.

Gorokhov, I. M., Kuznetsov, A. B., Melezhik, V. A., Konstantinova, G. V. & Melnikov, N. N. 1998. Sr isotope composition of upper Jatulian dolostones of the Tulomozero Formation, south-eastern Karelia. *Transactions of the Russian Academy of Sciences. Earth Sciences Sections (Geochemistry)* **360**, 533–6.

Handford, C. R. 1981. Coastal sabkha and salt pan deposition of the lower Clear Fork Formation (Permian), Texas. *Journal of Sedimentary Petrology* **51**, 761–78.

Hillaire Marcel, C. & Casanova, J. 1987. Isotopic hydrology and paleohydrology of the Magadi (Kenya)–Natron (Tanzania) Basin during the late Quaternary. *Palaeogeography, Palaeoclimatology, Palaeoecology* **58**, 155–81.

Hollander, D. J. & McKenzie, J. A. 1991. $CO_2$ control on carbon isotope fractionation during aqueous photosynthesis: a paleo-$pCO_2$ barometer. *Geology* **19**, 929–32.

Janaway, T. M. & Parnell, J. 1989. Carbonate production within the Orcadian Basin, northern Scotland; a petrographic and geochemical study. *In* Talbot, M. R. & Kelts, K. (eds) *The Phanerozoic record of lacustrine basins and their environmental signals. Palaeogeography, Palaeoclimatology, Palaeoecology* **70**, 89–105.

Jørgensen, B. B., Nelson, D. C. & Ward, D. M. 1992. Chemostratigraphy and decomposition in modern microbial mats. In: Schopf, J. W. & Klein, C. (eds) *The Proterozoic biosphere*, 287–93. Cambridge: Cambridge University Press.

Karhu, J. A. 1993. Palaeoproterozoic evolution of the carbon isotope ratios of sedimentary carbonates in the Fennoscandian Shield. *Geological Survey of Finland Bulletin* **371**, 1–87.

Karhu, J. A. & Holland, H. D. 1996. Carbon isotopes and the rise of atmospheric oxygen. *Geology* **24**, 867–79.

Karhu, J. A. & Melezhik, V. A. 1992. Carbon isotope systematics of early Proterozoic sedimentary carbonates in the Kola Peninsula, Russia: correlations with Jatulian formations in Karelia. *In* Balagansky, V. V. & Mitrofanov F. P. (eds) *Correlations of Precambrian formations of the Kola-Karelia region and Finland*, pp. 48–53. Apatity: Kola Scientific Centre of the Russian Academy of Sciences.

Katz, A., Kolodny, Y. & Nissenbaum, A. 1977. The geochemical evolution of the Pleistocene Lake Lisisan – Dead Sea system. *Geochimica et Cosmochimica Acta* **41**, 1609–26.

Kaufman, A. J. & Knoll, A. H. 1995. Neoproterozoic variations in the C-isotopic composition of seawater: stratigraphic and biogeochemical implications. *Precambrian Research* **73**, 27–49.

Kelts, K. & Hsü, K. J. 1978. Freshwater carbonate sedimentation. *In* Lerman, A. (ed.) *Lakes; chemistry, geology, physics*, 295–323. Berlin: Springer.

Koch, P. L. Zachos, J. C & Gingerich, P. D. 1992. Correlation between isotope records in marine and continental carbon reservoirs near the Palaeocene/Eocene boundary. *Nature* **358**, 319–22.

Land, L. S. 1992. The dolomite problem: stable and radiogenic isotope clues. *In* Clauer, N. & Chaudhuri, S. (eds) *Isotopic signatures and sedimentary records*, 49–68. Berlin: Springer-Verlag.

Levy, Y. 1977. The origin and evolution of brine in coastal sabkhas, northern Sinai. *Journal of Sedimentary Petrology* **47**, 451–62.

McCrea, J. M. 1950. On the isotopic chemistry of carbonates and a paleotemperature scale. *Journal of Chemical Physics* **18**, 849–57.

McKenzie, J. A. 1981. Holocene dolomitization of calcium carbonate sediments from the coastal sabkhas of Abu Dhabi, U.A.E.: a stable isotope study. *Journal of Geology* **89**, 185–98.

McKenzie, J. A. 1985. Carbon isotopes and productivity in the lacustrine and marine environment. *In* Stumm, W. (ed.) *Chemical processes in lakes*, 99–118. New York: Wiley.

McKenzie, J. A. & Eberli, G. P. 1987. Indications for abrupt Holocene climatic change; late Holocene oxygen isotope stratigraphy of the Great Salt Lake, Utah. *In* Berger, W. H. & Labeyrie, L. D. (eds) *Abrupt climatic change; evidence and implications. NATO ASI Series, Series C: Mathematical and Physical Sciences* **216**, 127–36.

Melezhik, V. A. 1992. *Palaeoproterozoic sedimentary and rock-forming basins of the Fennoscandian Shield*. Leningrad: Nauka. [In Russian.]

Melezhik, V. A., Fallick, A. E., Makarikhin, V. V. & Lubtsov, V. V. 1997. Links between Palaeoproterozoic palaeogeography and rise and decline of stromatolites: Fennoscandian Shield. *Precambrian Research* **82**, 311–48.

Melezhik, V. A., Fallick, A. E., Medvedev, P. V. & Makarikhin, V. V. 1999. Extreme $^{13}C_{carb}$ enrichment in ca. 2·0 Ga magnesite-stromatolite-dolomite-'red beds' association in a global context: a case for the world-wide signal enhanced by a local environment. *Earth-Science Reviews* **48** 71–120.

Melezhik, V. A., Fallick, A. E., Medvedev, P. V. & Makarikhin, V. V. 2000. Palaeoproterozoic magnesite-stromatolite-dolomite-'red beds' association, Russian Karelia: palaeoenvironmental constraints on the 2·0 Ga positive carbon isotope shift. *Norsk Geologisk Tidsskrift* **80**, 163–86.

Melezhik, V. A., Fallick, A. E., Smirnov, Yu. P & Yakovlev, Yu. N. 2003. Fractionation of carbon and oxygen isotopes in $^{13}C$-rich Palaeoproterozoic dolostones in the transition from medium-grade to high-grade greenschist facies: a case study from the Kola Superdeep Drillhole. *Journal of the Geological Society, London* **160** 71–82.

Melezhik, V. A. & Fallick, A. E. 1996. A widespread positive $\delta^{13}C_{carb}$ anomaly at around 2·33–2·06 Ga on the Fennoscandian Shield: A paradox? *Terra Nova* **8**, 141–57.

Melezhik, V. A. & Fallick, A. E. 1997. Paradox regained? Reply. *Terra Nova* **9**, 148–51.

Melezhik, V. A. & Fallick, A. E. 2001. Proterozoic travertines of volcanic affiliations from a $^{13}C$-rich rift lake environment. *Chemical Geology* **173**, 293–312.

Melezhik, V. A. & Fallick, A. E. 2003. $\delta^{13}C$ and $\delta^{18}O$ analyses of microcored samples: several contrasting examples from Palaeoproterozoic $^{13}C$-rich dolostones. *Chemical Geology* **201**, 213–28.

Melezhik, V. A. & Fallick, A. E. 2005. Palaeoproterozoic, rift-related, $^{13}C$-rich, lacustrine carbonates, NW Russia–Part I: Sedimentology and major element geochemistry. *Transactions of the Royal Society of Edinburgh: Earth Sciences* **95** (for 2004), 393–421.

Melezhik, V. A. & Sturt, B. A. 1994. General geology and evolutionary history of the early Proterozoic Polmak-Pasvik-Pechenga-Imandra/Varzuga-Ust'Ponoy Greenstone Belt in the north-eastern Baltic Shield. *Earth-Science Reviews* **36**, 205–41.

Morante, R., Veevers, J. J. Andrew, A. S. & Hamilton, P. J. 1994. Determination of the Permian–Triassic boundary in Australia from carbon isotope stratigraphy. *Journal of Australian Petroleum Exploration Association* **34**, 330–6.

Müller, D. W., McKenzie, J. A. & Mueller, P. A. 1990. Abu Dhabi Sabkha, Persian Gulf, revisited; application of strontium isotopes to test an early dolomitization model. *Geology* **18**, 618–21.

Neev, D. 1963. Recent precipitation of calcium salts in the Dead Sea. *Research Council of Israel Bulletin* **11G**, 153.

Nesbitt, H. W. 1990. Groundwater evolution, authigenic carbonates and sulphates of the Basque Lake No. 2 Basin, Canada. *In* Spenser, R. J. & Chou, I. M. (eds) *Fluid-mineral interactions; a tribute to H. P. Eugster. Geochemical Society Special Publication* **2**, 355–71.

Oberhänsli, H. & Allen, P. A. 1987. Stable isotopic signatures of Tertiary lake carbonates, Eastern Ebro Basin, Spain. *Palaeogeography, Palaeoclimatology, Palaeoecology* **60**, 59–75.

Ojakangas, R. W., Marmo, J. S. & Heiskanen, K. I. 2001. Basin evolution of the Paleoproterozoic Karelian Supergroup of the Fennoscandian (Baltic) Shield. *Sedimentology* **141–142**, 255–85.

O'Neil, J. R., Clayton, R. N. & Mayeda, T. K. 1969. Oxygen isotope fractionation in divalent metal carbonates. *Journal of Chemical Physics* **51**, 5547–58.

Palmer, M. R. & Edmond, J. M. 1989. The strontium isotope budget of the modern ocean. *Earth and Planetary Science Letters* **92**, 11–26.

Parry, W. T., Reeves, C. C., Jr & Leach, J. W. 1970. Oxygen and carbon isotopic composition of West Texas lake carbonates. *Geochimica et Cosmochimica Acta* **34**, 825–39.

Patterson, R. J. & Kinsman, J. J. 1982. Formation of diagenetic dolomite in coastal sabkha along Arabian (Persian) Gulf. *American Association of Petroleum Geologists Bulletin* **66**, 28–43.

Petrov, V. P. & Voloshina, I. M. 1995. Regional metamorphism of the Pechenga area rocks. *In* Mitrofanov, F. P. & Smol'kin, V. F. (eds) *Magmatism, sedimentogenesis and geodynamics of the Pechenga palaeorift*, pp. 164–82. Kola Science Centre, Apatity. [In Russian.]

Pokrovsky, B. G. & Melezhik, V. A. 1995. Variations of oxygen and carbon isotopes in Palaeoproterozoic carbonate rocks of the Kola Peninsula. *Stratigraphy and Geological Correlation* **3**, 42–53.

Reeves, C. C., Jr & Parry, W. T. 1965. Geology of West Texas pluvial lake carbonates. *American Journal of Science* **263**, 606–15.

Renaut, R. W. Tiercelin, J.-J. & Owen, R. B. 1986. Mineral precipitation and diagenesis in the sediments of the Lake Bogoria Basin, Kenya Rift valley. *In* Frostick, L. E., Renaut, R. W., Reid, I. & Tiercelin, J. J. (eds) *Sedimentation in the African rifts. Geological Society of London Special Publications* **25**, 159–75.

Renaut, R. W. & Owen, R. B. 1988. Opaline cherts associated with sublacustrine hydrothermal springs at Lake Bogoria, Kenya Rift Valley. *Geology* **16**, 699–702.
Renaut, R. W. & Tiercelin, J.-J. 1993. Lake Bogoria, Kenya: soda, hot springs and about a million flamingoes. *Geology Today* **9**, 56–61.
Ricketts, R. D. & Johnson, T. C. 1996. Early Holocene changes in lake level and productivity in Lake Malawi as interpreted from oxygen and carbon isotopic measurements of authigenic carbonates. *In* Johnson, T. C. & Odada, E. O. (eds) *The limnology, climatology and paleoclimatology of the East African lakes*, pp. 475–93. Australia: Gordon and Breach.
Rosen, M. R., Miser, D. E., & Warren, J. K. 1988. Sedimentology, mineralogy and isotopic analysis of Pellet Lake, Coorong region, South Australia. *Sedimentology* **35**, 105–22.
Rosenbaum, J. M. & Sheppard, S. M. F. 1986. An isotopic study of siderites, dolomites and ankerites at high temperatures. *Geochimica et Cosmochimica Acta* **50**, 1147–59.
Rothe, P., Hoefs, J. & Sonne, V. 1974. The isotopic composition of Tertiary carbonates from the Mainz Basin; an example of isotopic fractionations in 'closed basins'. *Sedimentology* **21**, 373–95.
Rothe, P. & Hoefs, J. 1977. Isotopen-geochemische Untersuchungen an Karbonaten der Ries-See-Sedimente der Forschungsbohrung Nördlingen 1973. *Geologica Bavarica* **75**, 59–66.
Schidlowski, M., Eichmann, R. & Junge, C. E. 1976. Carbon isotope geochemistry of the Precambrian Lomagundi carbonate province, Rhodesia. *Geochimica et Cosmochimica Acta* **40**, 449–55.
Schidlowski, M., Matzigkeit, U. & Krumbein, W. E. 1984. Superheavy organic carbon from hypersaline microbial mats; assimilatory pathway and geochemical implications. *Naturwissenschaften* **71**, 303–8.
Schoell, M. 1978. Oxygen isotope analyses on authigenic carbonates from Lake Van sediments and their bearing on the climate of the past 10,000 years. *In* Degens, E. T. & Kurtman, F. (eds) The geology of Lake Van. *Maden Tetkik ye Arama Enstituesue Yayinlarindan* **169**, 92–7.
Shields, G. 1997 A widespread positive $\delta^{13}C_{carb}$ anomaly at around 2·33–2·06 Ga on the Fennoscandian Shield. Comment: Paradox lost? *Terra Nova* **9**, 148.
Spencer, R. J., Baedecker, M. J., Eugster, H. P., Forester, R. M., Goldhaber, M. B., Jones, B. F., Kelts, K., McKenzie, J., Madsen, D. B., Rettig, S. L., Rubin, M & Bowser, C. J. 1984. Great Salt Lake, and precursors, Utah; the last 30,000 years. *Contributions to Mineralogy and Petrology* **86**, 321–34.
Stein, M., Starinsky, A., Katz, A., Goldstein, S. L., Machlus, M. & Schramm, A. 1997. Strontium isotopic, chemical, and sedimentological evidence for the evolution of Lake Lisan and the Dead Sea. *Geochimica et Cosmochimica Acta* **61**, 3975–92.
Stiller, M. & Hutchinson, G. E. 1980. The waters of Merom: a study of Lake Huleh. VI. Stable isotopic composition of carbonates of a 54 m core; paleoclimatic and paleotrophic implications. *Archiv für Hydrobiologie* **89**, 275–302.
Stiller, M. & Kaufman, A. 1985. Paleoclimatic trends revealed by the isotopic composition of carbonates in Lake Kinneret. *In* Kuhn, M. (ed.) *Climate and paleoclimate of lakes, rivers and glaciers. Zeitschrift fuer Gletscherkunde und Glazialgeologie* **21**, 79–87.
Stiller, M. & Magaritz, M. 1974. Carbon-13 enriched carbonate in interstitial waters of Lake Kinneret sediments. *Limnology and Oceanography* **19**, 849–53.
Stuiver, M. 1970. Oxygen and carbon isotope ratios of fresh-water carbonates as climatic indicators. *Journal of Geophysical Research* **75**, 5247–57.
Suchecki, R. K., Hubert, J. F. & Birney de Wet, C. C. 1988. Isotopic imprint of climate and hydrogeochemistry on terrestrial strata of the Triassic-Jurassic Hartford and Fundy rift basins. *Journal of Sedimentary Petrology* **58**, 801–11.
Talbot, M. R. 1990. A review of the palaeohydrological interpretation of carbon and oxygen isotopic ratios in primary lacustrine carbonates. *Chemical Geology* **80**, 261–79.
Talbot, M. R. & Kelts, K. 1990. Paleolimnological signatures from carbon and oxygen isotopic ratios in carbonates from organic carbon-rich lacustrine sediments. *In* Katz, B. J. (ed.) *Lacustrine basin exploration; case studies and modern analogs. American Association of Petroleum Geologists Memoir* **50**, 99–112.
Tietze, K., Geyh, B., Mueller, H., Schroeder, L., Stahl, W. & Werner, H. 1980. The genesis of the methane in Lake Kivu (Central Africa). *Geologische Rundschau* **69**, 452–72.
Tikhomirova, M. & Makarikhin, V. V. 1993. Possible reasons for the $\delta^{13}C$ anomaly of lower Proterozoic sedimentary carbonates. *Terra Nova* **5**, 244–8.
Trichet, J., Defarqe, C. Tribble, J., Tribble, G. & Sansone, F. 2001. Christmas Island lagoonal lakes, models for the deposition of carbonate-evaporite-organic laminated sediments. *Sedimentary Geology* **140**, 177–89.
Turner, J. V. & Fritz, P. 1983. Enriched $^{13}C$ composition of interstitial waters in sediments of a freshwater lake. *Canadian Journal of Earth Sciences* **20**, 616–21.
Turovskiy, D. S. & Sheko, A. B. 1973. New data on the formation of carbonates in Lake Balkhash. *Lithology and Mineral Resources* **5**, 33–45. [In Russian.]
Utrilla, R., Vazquez, A. & Anadon, P. 1998. Paleohydrology of the upper Miocene Bicorb Lake (eastern Spain) as inferred from stable isotopic data from inorganic carbonates. *Sedimentary Geology* **121**, 191–206.
Vasconcelos, C. & McKenzie, J. A. 1997. Microbial mediation of modern dolomite precipitation and diagenesis under anoxic conditions (Lagoa Vermelha, Rio de Janeiro, Brazil). *Journal of Sedimentary Research* **67**, 378–90.
Veizer, J. 1989. Strontium isotopes in seawater through time. *Annual Review of Earth and Planetary Sciences* **17**, 141–67.
Veizer, J. & Compston, W. 1974. $^{87}Sr/^{86}$ Sr composition of seawater during the Phanerozoic. *Geochimica et Cosmochimica Acta* **38**, 1461–84.
Wadleigh, M. A., Veizer, J. & Brooks, C. 1985. Strontium and its isotopes in Canadian rivers; fluxes and global implications. *Geochimica et Cosmochimica Acta* **49**, 1727–36.
Winkler, H. G. F. 1979. *Petrogenesis of metamorphic rocks*. Berlin: Springer-Verlag.
Yudovich, Ya. E., Makarikhin, V. V., Medvedev, P. V. & Sukhanov, N. V. 1991. Carbon isotope anomalies in carbonates of the Karelian Complex. *Geochemica International* **28**, 56–62.

V. A. MELEZHIK, Geological Survey of Norway, Leiv Erikssons vei 39, N-4791, Trondheim, Norway.

A. E. FALLICK, Scottish Universities Environmental Research Centre, East Kilbride, Glasgow G75 0QF, Scotland.
e-mail: T.Fallick@suerc.gla.ac.uk

A. B. KUZNETSOV, Institute of Precambrian Geology and Geochronology, nab. Makarova 2, 199034 St Petersburg, Russia.

MS received 22 April 2003. Accepted for publication 12 May 2004.